Senescence in Temperate Broadleaf Trees Exhibits Species-Specific Dependence on Photoperiod versus Thermal Forcing

Minkyu Moon[1*], Andrew D. Richardson[2,3], John O'Keefe[4], and Mark A. Friedl[1]

[1]Department of Earth and Environment, Boston University, USA

[2]School of Informatics, Computing, and Cyber Systems, Northern Arizona University, USA

[3]Center for Ecosystem Science and Society, Northern Arizona University, USA

[4]Harvard Forest, Harvard University, USA

*Corresponding author: 685 Commonwealth Avenue, Boston, MA 02215, USA

E-mail address: moon.minkyu@gmail.com (Minkyu Moon)

Abstract

Incomplete understanding of the processes controlling senescence limits our ability to forecast how the timing of leaf senescence will change in coming decades. In this study, we use a hierarchical Bayesian model (HBM) in association with a 27+ year record of field observations for 12 temperate deciduous tree species collected at Harvard Forest in central Massachusetts to examine how variability in bioclimatic controls affects the timing of leaf senescence. To test how general and extensible our results are over a broader biogeographic range, we used a multi-year record of land surface phenology derived from remote sensing encompassing all forested lands in New England. Results from the HBM showed that while air temperature is an important factor that influences the timing of leaf senescence, photoperiod uniformly exerts the strongest control across all 12 species. Species exhibiting the strongest dependence on photoperiod, particularly *Acer* species, showed low inter-annual variation and no long-term trends in the timing of leaf senescence. In contrast, species with greater dependence on air temperature, particularly *Quercus* species, showed statistically significant trends toward later senescence dates in response to long-term warming. Results from analyses conducted at regional scale across all of New England using data derived from remote sensing corroborated results obtained at Harvard Forest. Specifically, relative to ecoregions dominated by *Quercus* species, the timing of leaf senescence in ecoregions dominated by *Acer* species exhibited lower interannual variability and lower correlation with year-to-year variation in pre-senescence period mean air temperatures. These results suggest that forecasting how the timing of leaf senescence in temperate forests will change in the future requires species-specific understanding of how bioclimatic forcing controls the timing of leaf senescence.

Keywords: leaf senescence, temperate deciduous forests, photoperiod, temperature sensitivity, Bayesian, hierarchical modeling

1. Introduction

The seasonality of vegetation activity influences a wide array of ecosystem functions (Bonan, 2008). Hence, understanding how ecological and bioclimatic processes control vegetation phenology is critical to understanding how ecosystems will respond to future climate change (Buermann et al., 2018; Piao et al., 2019; Richardson et al., 2018). However, despite extensive efforts devoted to this topic, mechanistic understanding of what controls plant phenology remains incomplete (Delpierre et al., 2016; Zohner et al., 2016). In this context, a large proportion of phenological research has focused on the mechanisms that control the timing of leaf emergence, while understanding of the eco-physiological processes that control leaf senescence is less well-developed (Chen et al., 2020; Vitasse et al., 2021; Zani et al., 2020).

A key challenge in developing comprehensive understanding and models of fall phenology is that, unlike in spring, senescence is preceded by a growing season that typically spans several months. Hence, the mechanisms and processes that control leaf senescence are potentially more complex than those controlling spring phenology, which increases the challenges involved in understanding of how senescence will respond to ongoing climate change. For example, previous studies have suggested that both genetic factors (Friedman et al., 2011) and changes in bioclimatic variables throughout the growing season influence the timing of senescence (Bigler and Vitasse, 2021; Chen et al., 2020; Wu et al., 2018; Y. Zhang et al., 2020). Variation in the timing of leaf senescence impacts seasonal-scale ecosystem productivity by regulating the length of growing season (Park et al., 2016; Zani et al., 2020) and nutrient status of individual trees and at the ecosystem-scale (Dox et al., 2020; Havé et al., 2017), and can also affect important ecological processes such as the timing of reproduction for many plant and animal species (Gallinat et al., 2015; Renner and Zohner, 2018). Therefore, improved understanding of the processes that control

leaf senescence is needed to understand how vegetation phenology will change in the coming decades and to improve forecasts of how ecosystem functions that are affected by leaf senescence will be impacted by these changes.

The two bioclimatic factors that are most widely assumed to control the timing of leaf senescence are air temperature and day-length (*i.e.*, photoperiod), both of which tend to decrease prior to leaf senescence in extra-tropical ecosystems (Fu et al., 2018; Gill et al., 2015; Keskitalo et al., 2005; Lang et al., 2019; Liu et al., 2020). As a result, most models use air temperature and photoperiod as the primary drivers of leaf senescence (Peano et al., 2021). In recent years, a variety of research has identified a suite of additional factors that may influence the timing of senescence including the rate and amount of photosynthesis prior to senescence onset (Zani et al., 2020), water stress (Peng et al., 2019; Xie et al., 2018), the timing of leaf emergence in spring (Keenan and Richardson, 2015; Peng et al., 2021), and plant and soil nutrient status (Estiarte and Peñuelas, 2015; Keskitalo et al., 2005). Further, several recent studies have reported that daily minimum and maximum air temperatures may have differing influence on the timing of leaf senescence (Meng et al., 2020; Wu et al., 2018). However, there is no current consensus regarding how environmental drivers control the onset of leaf senescence in temperate broadleaf forests.

A key quandary from previous studies, that has been known for nearly a decade, is that results from lab- and field-based experimental studies that have been explicitly designed to identify phenological sensitivity to climate forcing differ from patterns observed in natural ecosystems arising from climate variability (Leuzinger et al., 2011; Primack et al., 2015; Vitasse et al., 2014; Wolkovich et al., 2012; but see Hänninen et al., 2019). Further, the limited spatial and temporal coverage of these studies, which are generally conducted at local scales with study areas less than 10 km^2 and time scales shorter than 10 years, is a significant limitation that inhibits their ability to

provide general results. As a solution, process-based phenological models calibrated to both *in-situ* and remote sensing-based observations of phenology have been widely used to make inferences and advance understanding of the ecological and environmental factors that control phenological events such as the start of senescence (Delpierre et al., 2009; Lang et al., 2019; Liu et al., 2020; Schaber and Badeck, 2003). Unfortunately, however, the models used in these studies include two fundamental limitations: (1) they prescribe functional relationships among forcing variables and phenological events based on incomplete understanding; and (2) the most widely-used functional forms of these models use parameters that have been aggregated over time periods that span weeks-to-months (*e.g.*, growing degree days) and do not capture short-term variability that is increasingly recognized to have a significant impact on phenological behavior (Clark et al., 2014b; Moon et al., 2021b).

To address both the knowledge gaps and limitations of models described above, and specifically focusing on how environmental drivers control the timing of leaf senescence in temperate forests, here we use a data-driven hierarchical Bayesian model (HBM) estimated using long-term field measurements of bioclimatic forcing and leaf senescence dates for 12 temperate deciduous tree species in New England. To compare our results against a state-of-the-art process-based model, we also tested the model described by Caffarra et al. (2011), which incorporates the effects of photoperiod, air temperature, and anomalies in the timing of leaf unfolding. Using these models, we assessed their ability to explain species-specific differences in the sensitivity of fall phenology to climate forcing. To evaluate our results and conclusions at a broader geographic scale, we linked the site-level and species-specific patterns that we estimate using the HBM to regional-scale patterns and trends in the timing of senescence of temperate forests across all of

New England using species density maps and large-scale records of land surface phenology from remote sensing.

2. Methods and Data

2.1. Field observations

Phenological observations of woody plants have been recorded since 1990 to the present at the Harvard Forest, a long-term ecological research site located in Petersham Massachusetts (42.53° N, 72.18° W; Fig. S1) (O'Keefe, 2019). Each of the trees included in the survey is located within 1.5 km of the Harvard Forest headquarters at elevations between 335 and 365 m above sea level. For fall phenology, weekly observations of percent leaf coloration and percent leaf fall are recorded from the beginning of September to the end of leaf fall each year. In this study, we used data characterizing the timing of leaf coloring for 12 species, all of which have at least 20 years of observations over the 28 year period from 1992-2019 (*Acer pensylvanicum* (ACPE), *Acer rubrum* (ACRU), *Acer saccharum* (ACSA), *Amelanchier alnifolia* (AMAF), *Betula alleghaniensis* (BEAL), *Betula lenta* (BELE), *Betula papyrifera* (BEPA), *Fraxinus americana* (FRAM), *Prunus serotina* (PRSE), *Quercus alba* (QUAL), *Quercus rubra* (QURU), and *Quercus velutina* (QUVE); Table S1). Leaf coloring date is defined as the day of year (DOY) on which 50% of the leaves have changed color on an individual tree. Typically, three to five individuals of each species are observed in each year, with different individuals observed in different years (Table S2). Our analysis also used budburst date for the same trees, which is defined as the DOY when 50% of the buds on the tree have recognizable leaves emerging from them (see Section 2.3). Sub-weekly observations would be useful to help resolve rapidly changing phenological processes (*e.g.*, Gao et al., 2017; Keenan et al., 2014). However, numerous studies have used these data to estimate

127 models and analyze trends in phenology at Harvard Forest (*e.g.*, Archetti et al., 2013; Dunn et al.,
128 2021; Richardson et al., 2006), which demonstrates that these data provide a sound basis for
129 phenological studies. Measurements of carbon fluxes and daily meteorology were obtained from
130 the Harvard Forest Environmental Monitoring Station (EMS) eddy covariance tower (Munger and
131 Wofsy, 2020).

132

133 *2.2. Modeling long-term trends in leaf senescence*

134 In the first element of our analysis, we estimated species-specific long-term trends in the timing
135 of leaf senescence. To do this, we used the non-parametric Theil-Sen estimator to estimate the
136 trend for each tree species (Sen, 1968), and distinguished species with statistically significant
137 trends ($p < 0.05$) from those not showing trends using the Mann-Kendall test (Mann, 1945). We
138 also estimated long-terms trends in air temperatures measured at the EMS tower using the same
139 approach for each of annual, late summer (from August to October; *i.e.*, directly prior to leaf
140 senescence), and spring (from March to May) time periods.

141

142 *2.3. Hierarchical Bayesian model of leaf senescence*

143 To estimate the sensitivity of leaf senescence timing to bioclimatic controls, we used a
144 hierarchical Bayesian model (HBM) estimated using the field observations described in Section
145 2.1. The original form of this model was proposed by Clark et al. (2014b, 2014a), and Moon et al.
146 (2021b) recently adapted it to model springtime phenology at large spatial scale using remote
147 sensing. The HBM has two main advantages for the analysis we describe here. First, because the
148 relative importance among bioclimatic controls that affect the timing of senescence is estimated

by data itself, the HBM does not suffer from issues related to model misspecification related to prescribed functional relationships among control variables that are embedded in conventional process-based models (see Peano et al. (2021) and Section 2.4). Second, the HBM is estimated using daily data and so is able to capture the continuous response of phenological processes to both short- and long-term variation in environmental forcing (Clark et al., 2014b, 2014a; Moon et al., 2021b).

The HBM uses a state-space framework that includes an unobserved latent state h to continuously track the response of phenological processes to environmental forcing at daily time step. In this framework, changes in the latent state (h) are computed as:

$$h_{d+1} = h_d + \delta h_d \quad (1)$$

where h_d is the latent state on day d. δh_d is the change in h from day d to day $d + 1$, which is estimated as:

$$\delta h_d = \begin{cases} (X_d\beta)(1 - h_d/h_{max}), & \delta h_d \geq 0 \\ 0, & \delta h_d < 0 \end{cases} \quad (2)$$

where X_d is a matrix of predictors that includes daily meteorological forcing variables (air temperature, photoperiod, vapor pressure deficit (VPD), and photosynthetically active radiation (PAR)), along with species-specific budburst dates and early-season gross primary productivity (GPP) derived from eddy covariance measurements at the Harvard Forest EMS tower. Here, we define early-season GPP as the accumulated daily GPP from May 1 to July 31, which nominally corresponds to the first half of the growing season. β is a vector of estimated model coefficients (*i.e.*, posterior distributions from the model). Note that because the input data (X_d) are normalized (*i.e.*, to have a mean of 0 and a standard deviation of 1 for each of the input variables) prior to

model estimation, the magnitudes of each model coefficient, which reflect the dependence of senescence development on each input variable (*i.e.*, β), are independent of the magnitude and units of each input variable (and hence can be compared). h_{max} is the final state value of h, and is prescribed to be 100.

To link the continuous scale of the latent state h to a form that identifies discrete phenological events (*i.e.*, recorded dates of leaf senescence), we use a logit transformation:

$$logit(P_d) = \kappa + \lambda \times h_d \quad (3)$$

where P_d is the probability that leaf senescence occurs on day d, and κ and λ are the intercept and slope of the transformation, respectively. Because the leaf senescence date is defined to be a discrete event, P_d follows a Bernoulli distribution:

$$Y_d \sim Bernoulli(P_d) \quad (4)$$

where Y_d indicates whether leaf senescence has occurred on day d (*i.e.*, 1 or 0).

2.4. Model estimation and evaluation

To estimate the HBM, we used the median date of leaf senescence in each year from observations of 3 to 5 individual trees, which yielded a 28-year time series of leaf senescence dates for each species except QURU, which had a 27-year record (Table S2). Using these data, we estimated the HBM for six different sets of bioclimatic variables with two main goals: (1) to quantify the relative importance of each variable in controlling in the timing of leaf senescence; and (2) to assess whether daily minimum and maximum air temperatures have distinct roles in controlling the timing of leaf senescence relative to mean daily temperature (see Meng et al., 2020;

187 Wu et al., 2018). To this end, we estimated six distinct HBMs using different combinations of (1)
188 daily mean air temperature, (2) daily minimum air temperature, (3) daily maximum air temperature,
189 (4) daily minimum and maximum air temperatures, and (5) daily mean air temperature and daily
190 temperature range, along with photoperiod, VPD, PAR, species-specific budburst dates, and early-
191 season GPP as predictor variables (hereafter, models M1-M5, respectively). Further, to assess the
192 role and importance of photoperiod in controlling the timing of leaf senescence, we estimated the
193 HBM using daily mean air temperature with all other variables, excluding photoperiod (model
194 M6). Each models' performance was evaluated based on the root-mean-square error (RMSE),
195 mean absolute error (MAE), and deviance information criterion (DIC). Posterior sampling was
196 performed using the 'R2jags' package in R (Su and Yajima, 2015), with 10,000 iterations and
197 3,000 burn-in periods for each model.

198 In addition, to evaluate the HBM's performance against a state-of-the-art of process-based leaf
199 senescence model, we used the Harvard Forest data set to estimate the model described by Caffarra
200 et al. (2011) (hereafter CSM). We chose the CSM for this comparison based on recent results from
201 Liu et al., (2020), who used multiple widely used process-based leaf senescence models in
202 association with over 19,000 site-years of *in-situ* phenological records covering four temperate
203 deciduous tree species in Europe to show that the CSM performed best among the models they
204 used, especially in capturing interannual variation in leaf senescence dates. The CSM hypothesizes
205 that the progression of leaf senescence, which is defined as the dormancy induction state DS, is
206 negatively related to both air temperature and photoperiod via sigmoidal relationships.
207 Specifically, daily accumulation of DS is controlled by air temperature and photoperiod as follows:

$$DS(d) = \sum_{d_0}^{d} \frac{1}{1 + e^{aD(T_{(d)} - bD)}} \times \frac{1}{1 + e^{cD(P_{(d)} - P_{crit})}} \quad (5)$$

where d_0 is the start date of dormancy induction, which we prescribed as September 1st, and aD, bD, and cD are model coefficients. Leaf senescence occurs when the accumulated forcing (*i.e.*, $DS(d)$) reaches a critical threshold D_{crit}, which is a function of the anomaly in springtime phenology S_a:

$$D_{crit} = \alpha + \gamma \times S_a \quad (6)$$

where α and γ are parameters regulating the effects of changes in springtime phenology. For this study, we used the budburst dates collected at Harvard Forest as a proxy of springtime phenology. Parameters were optimized to minimize the RMSE in predicted versus observed senescence dates for each of the 12 species following the method described by Nelder and Mead (1965).

Lastly, to assess how the relative dependence on photoperiod versus air temperature (*i.e.*, the two dominant factors controlling in the timing of leaf senescence; see the Results) estimated by the HBM affect year-to-year variation in the timing of leaf senescence, we calculated the difference between the posterior distributions of photoperiod and air temperature (*i.e.*, $\beta_P - \beta_T$) for each species (n = 12), and used standard major axis regression to assess the magnitude of covariance between $\beta_P - \beta_T$ and interannual variation in leaf senescence dates.

2.5. Remote Sensing Data

To expand and generalize our analysis to regional scale, we used Version 1.1 of the Multi-Source Land Surface Phenology product (MSLSP30NA) (Friedl, 2021). This data product

provides yearly observations of phenophase transition dates at 30 m spatial resolution for North America for 2016-2020. Using time series of the two-band enhanced vegetation index (EVI2; Jiang et al., 2008) estimated from Harmonized Landsat 8 and Sentinel-2 (HLS) imagery (Claverie et al., 2018), the MSLSP30NA product retrieves the timing of seven phenophase transition dates for each growing season at each 30 m pixel (Bolton et al., 2020). To identify the timing of leaf senescence we used the MSLSP30NA mid-greendown date, which corresponds to the DOY when EVI2 time series pass below 50% of the EVI2 amplitude during the greendown phase. More specifically, we used mid-greendown dates for all deciduous broadleaf or mixed forest pixels in New England according to the 2016 USGS National Land Cover Database (USGS and Rigge, 2019), which includes 40 Level IV EPA ecoregions (Fig. S1).

We used the MSLSP30NA data set to perform two analyses designed to assess whether species-specific results obtained from in-situ observations at Harvard Forest generalize at regional scale. First, because the remote sensing time series is short and it is computationally infeasible to run the HBM at every pixel in New England, we examined the relationship between anomalies in the timing of senescence dates and mean air temperature in the pre-senescence period, which we defined as DOY 231 to 270 based on results from the HBM at Harvard Forest (Fig. S2). Second, we calculated the standard deviation (SD) in the timing of senescence at each 30-m pixel across the available time series for all forested pixels in New England. Using these data, we estimated a multiple linear regression using the basal area for *Acer* and *Quercus* species in each ecoregion as independent variables (*i.e.*, the total basal area for all three species for each of *Acer* and *Quercus* in each EPA ecoregion) and the standard deviation of senescence dates across years in each ecoregion as the dependent variable. For the species-specific basal areas, we used a gridded dataset

248 provided by the USDA Forest Service derived from satellite imagery in conjunction with extensive
249 field plot data providing tree species basal area (Wilson et al., 2013).

250

251 **3. Results**

252 Since 1992, annual mean air temperature at Harvard Forest has increased by 0.034 ºC per year
253 (p = 0.035), resulting in a total increase of 0.95 ºC over the past 30 years (Fig. S3a). During late
254 summer, when the impact of changes in bioclimatic variables on the timing of leaf senescence is
255 most pronounced (Fig S2), the warming trend was even stronger (0.059 ºC per year; Fig. S3b).
256 Inspection of long-term trends in the timing of senescence in response to this warming indicates
257 that the response of trees was species-specific (Fig. 1). Specifically, four of the twelve species
258 included in our analysis showed statistically significant trends towards later senescence onset dates
259 (QUVE, QURU, PRSE, and ACPE (see Fig. 1 for full species names); p-value < 0.05), with trends
260 that range from 0.18 days per year to 0.30 days per year, corresponding to a total shift of 5.0-8.4
261 days towards later onset of senescence dates over the 28-year study period. Among the species
262 showing non-significant trends, five species (ACRU, BEAL, BELE, PRSE, and QUAL) showed
263 positive trends (*i.e.*, later senescence), two species (ACSA and BEPA) showed negative trends,
264 and one species (AMAF) showed no trend. These results identify species-specific responses to
265 identical bioclimatic forcing over three decades,.

266

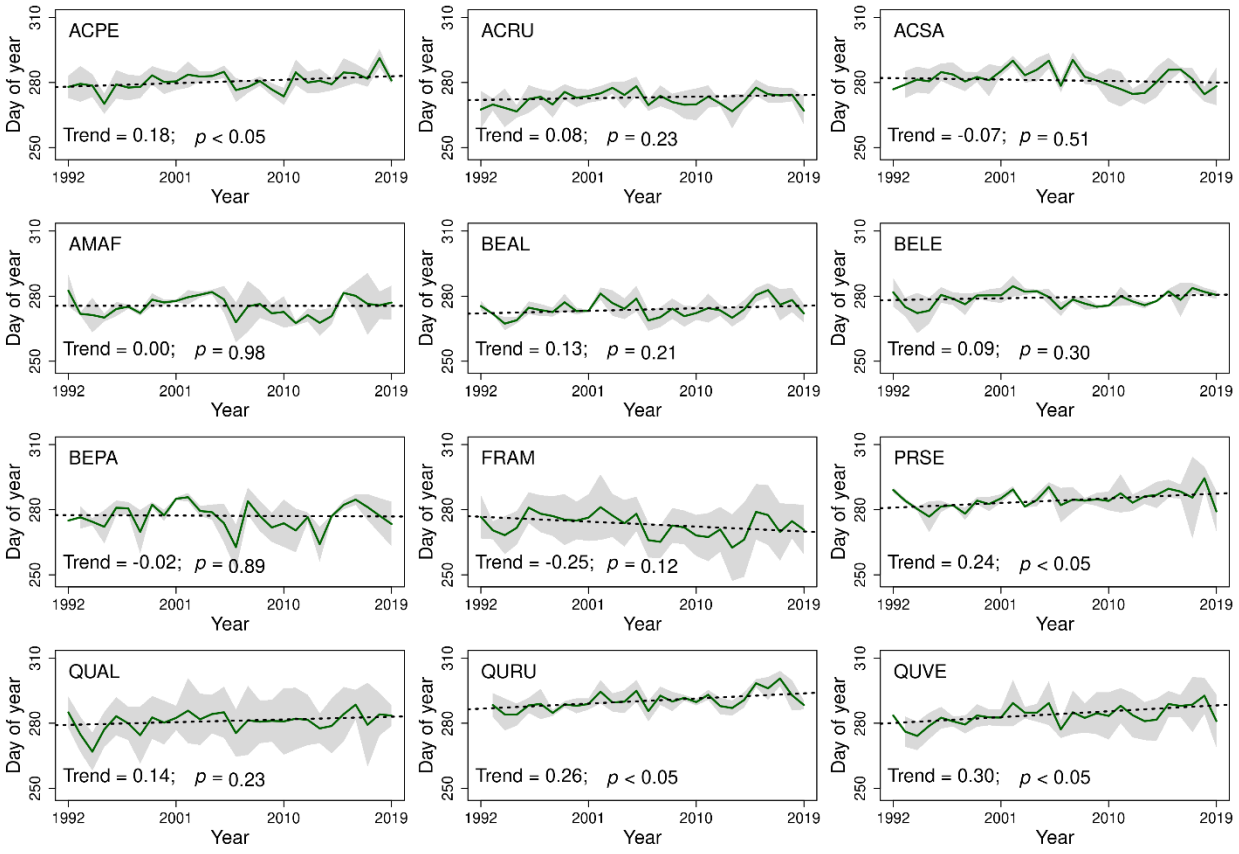

Fig. 1. Leaf coloration dates at Harvard Forest from 1992 to 2019. Solid green lines and shaded areas represent the annual mean and standard deviation in leaf coloration dates, respectively. Black dashed lines show the long-term trend (based on the Theil-Sen estimator) in days per year. APCE: *Acer pensylvanicum*; ACRU: *Acer rubrum*; ACSA: *Acer saccharum*; AMAF: *Amelanchier alnifolia*; BEAL: *Betula alleghaniensis*; BELE: *Betula lenta* BEPA: *Betula papyrifera*; FRAM: *Fraxinus americana*; PRSE: *Prunus serotina*; QUAL: *Quercus alba*; QURU: *Quercus rubra*; QUVE: *Quercus velutina*.

We tested six versions of the HBM using different combinations of bioclimatic predictor variables (Table 1). Overall, RMSEs and MAEs were low (ranging from 2.84 to 5.15 days and

from 2.21 to 4.14 days, on average, respectively), suggesting that the models realistically capture the eco-physiological response of deciduous trees to bioclimatic forcing during the leaf senescence phase. Among the different models, M5, which uses daily mean air temperature and daily air temperature range as predictors along with all the other variables, exhibited the best performance across all three model performance metrics. It's worth noting that model M6, which does not include photoperiod as a predictor, showed substantially worse predictive accuracy relative to the other five models. Scatterplots showing modeled versus observed leaf senescence dates provide visual corroboration that the HBM accurately predicts the observed timing of leaf senescence across all 12 species and demonstrates that the HBM predicts interannual variation in the timing of senescence (*e.g.*, QURU) with substantially more accuracy and realism than the CSM for all 12 species (Fig. 2; Table S3). Based on these results, hereafter we use model M5 for the rest of our analyses.

Table 1 Hierarchical Bayesian model performance statistics. M1-M6 refer to models using different sets of predictors: models M1-M5 use daily mean air temperature, daily minimum air temperature, daily maximum air temperature, daily minimum and maximum air temperatures, and daily mean air temperature and daily temperature range as predictor variables, along with photoperiod, vapor pressure deficit, photosynthetically active radiation, species-specific budburst dates, and early-season gross primary productivity; model M6 uses daily mean air temperature and includes all other variables except photoperiod. RMSE: root-mean-square error; MAE: mean absolute error; DIC: deviance information criterion. See Fig. 1 for definitions of species acronym.

Species	RMSE						MAE						DIC					
	M1	M2	M3	M4	**M5**	**M6**	M1	M2	M3	M4	**M5**	**M6**	M1	M2	M3	M4	**M5**	**M6**
ACPE	2.76	2.38	3.21	2.32	2.35	4.87	2.04	1.86	2.29	1.82	1.79	4.04	284	256	329	252	251	525
ACRU	2.54	2.55	2.83	2.61	2.48	5.57	1.89	1.93	2.11	1.96	1.93	4.64	285	278	298	280	281	592
ACSA	3.83	3.86	3.96	3.77	3.90	6.43	3.11	3.04	3.29	2.96	3.11	5.14	415	417	416	420	419	638
AMAF	3.15	3.23	3.23	3.27	3.08	5.22	2.46	2.86	2.46	2.61	2.46	4.21	335	343	344	342	336	534
BEAL	2.19	2.04	2.48	2.04	1.98	4.77	1.79	1.64	2.07	1.68	1.57	4.00	234	209	264	211	217	478
BELE	2.10	2.35	2.35	2.21	2.08	4.40	1.57	1.61	1.96	1.61	1.54	3.57	241	249	261	246	245	476
BEPA	4.90	4.62	5.04	4.80	4.73	6.18	3.89	3.61	4.07	3.61	3.54	4.82	502	486	519	489	493	655
FRAM	3.52	3.51	3.71	3.52	3.45	6.32	2.96	2.93	3.04	2.86	2.75	4.75	385	365	395	389	375	622
PRSE	2.57	2.57	2.71	2.54	2.58	5.07	2.18	2.04	2.18	2.04	2.07	3.86	278	318	293	333	275	516
QUAL	2.66	2.92	2.76	2.72	2.66	4.85	1.93	2.18	2.14	2.04	1.93	3.89	291	306	303	293	293	494
QURU	2.59	2.43	2.69	2.53	2.45	3.98	2.04	1.96	2.15	2.04	2.00	3.33	263	257	277	260	263	403
QUVE	2.45	2.46	2.62	2.41	2.41	4.13	1.79	1.86	2.07	1.68	1.82	3.43	272	347	285	366	272	428
Average	2.94	2.91	3.13	2.90	**2.84**	**5.15**	2.30	2.29	2.49	2.24	**2.21**	**4.14**	315	319	332	323	**310**	**530**

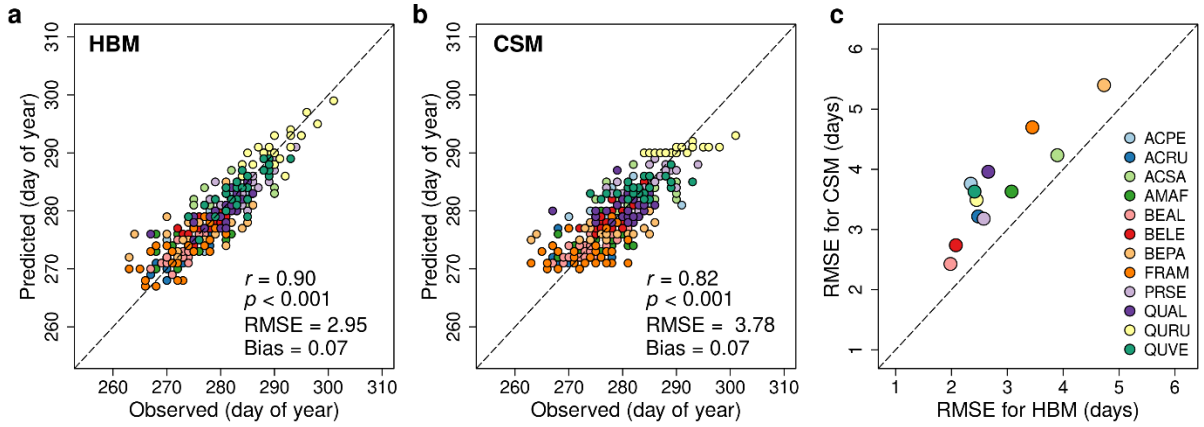

Fig. 2. Observed versus predicted leaf senescence dates across 12 deciduous tree species from (a) the Hierarchical Bayesian Model of leaf senescence and (b) the CSM model, and (c) comparison of RMSE's from each model. See Fig. 1 for definitions of species acronyms.

Results from the HBM indicate that air temperature and photoperiod are the two most important factors that control the timing of senescence (Fig. 3). Significantly, however, and consistent with results presented above examining long term trends in the timing of senescence, HBM results also show that the relative dependence of senescence on each of these controls is species-specific. Negative dependences indicate that decreases in the forcing variable prior to leaf senescence increase the probability of senescence. Hence, stronger negative dependence on air temperature and photoperiod relative to other variables reflect the fact that seasonal variation in air temperature and photoperiod (*i.e.*, cooling and shorter day-length, respectively) are the dominant factors that control the timing of leaf senescence. Relative to air temperature and photoperiod, the impact of the other variables included in the model (daily range of air temperature, VPD, PAR, budburst dates, and spring GPP) is modest. In this context, two key features are worth noting. First, across all 12 species, dependence on photoperiod is stronger than dependence on air temperature. Second, even though its overall effect is quite modest, the timing of leaf senescence exhibits mostly positive dependence on daily air temperature range, suggesting that larger amplitudes in daily air temperature promote earlier leaf senescence dates.

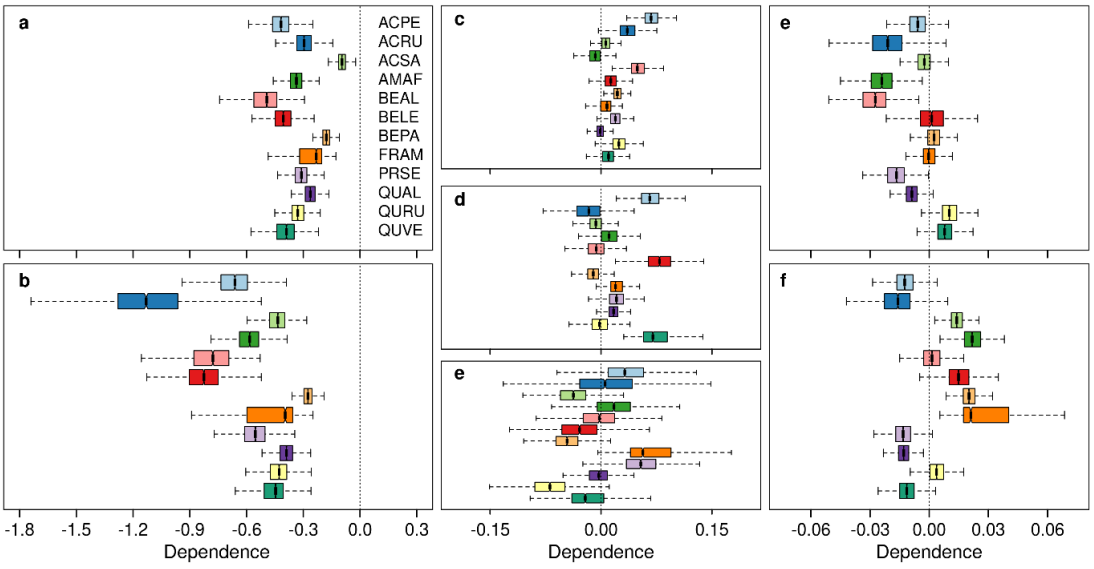

323

324 **Fig. 3.** Dependence of leaf senescence date on (a) daily mean air temperature, (b) photoperiod, (c)
325 daily range in air temperature, (d) daily mean vapor pressure deficit, (e) daily mean
326 photosynthetically active radiation, (f) budburst dates, and (g) early-season gross primary
327 productivity. Note that the magnitude of dependence in each column is different and decreases
328 from left to right. See Fig. 1 for definitions of species acronym.

329

330 Covariation between the magnitude of interannual variation in leaf senescence dates and
331 differences in the magnitude of photoperiod (β_{P}) and air temperature (β_{T}) dependence shows
332 strong correlation (Fig. 4). This result provides additional empirical evidence that stronger species-
333 specific dependence on photoperiod (air temperature) leads to smaller (larger) interannual
334 variation in leaf senescence dates. For example, on average, *Acer* species, which show larger
335 photoperiod dependence compared to other species, exhibit lower magnitudes of interannual
336 variation in senescence dates, whereas *Quercus* species, which show the weakest dependence on

photoperiod (*i.e.*, relatively greater dependence on temperature compared to *Acer* species), exhibit larger magnitudes of interannual variation.

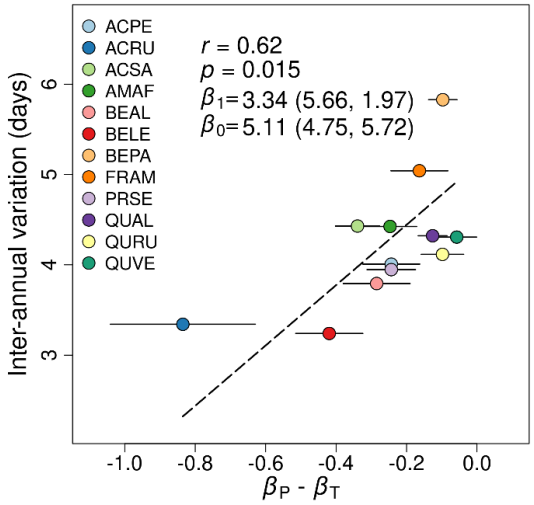

Fig. 4. Relationship between interannual variation in the timing of leaf senescence and the difference between photoperiod (β_P) and air temperature (β_T) dependence estimated by the HBM. The points and horizontal bars present the median ± one standard deviation, respectively, in the posterior distributions. The dashed line shows the standard major axis regression (SMA). SMA slope (β_1) and intercept (β_0) coefficients are provided with 95% confidence intervals. See Fig. 1 for definitions of species acronyms.

Land surface phenology data from remote sensing capture geographic patterns in the timing of leaf senescence at regional scale that are consistent with species-level patterns at Harvard Forest shown in Fig. 4 (Fig. 5). Specifically, eco-regions in New England where *Acer* species are more abundant show lower interannual variability in the timing of leaf senescence relative to areas dominated by *Quercus* species (Figs. 5a and S4a). Further, *Quercus*-dominant regions showed

greater sensitivity to pre-senescence period mean air temperature (*i.e.*, stronger dependence on air temperature), while *Acer*-dominant regions showed weaker sensitivity (Figs. 5b and S4b). Reinforcing this, results from a multiple linear regression using the basal area of *Acer* and *Quercus* species as predictors explained 63% of interannual variation in the timing of leaf senescence across the 40 EPA Level IV ecoregions in New England (Fig. 5d).

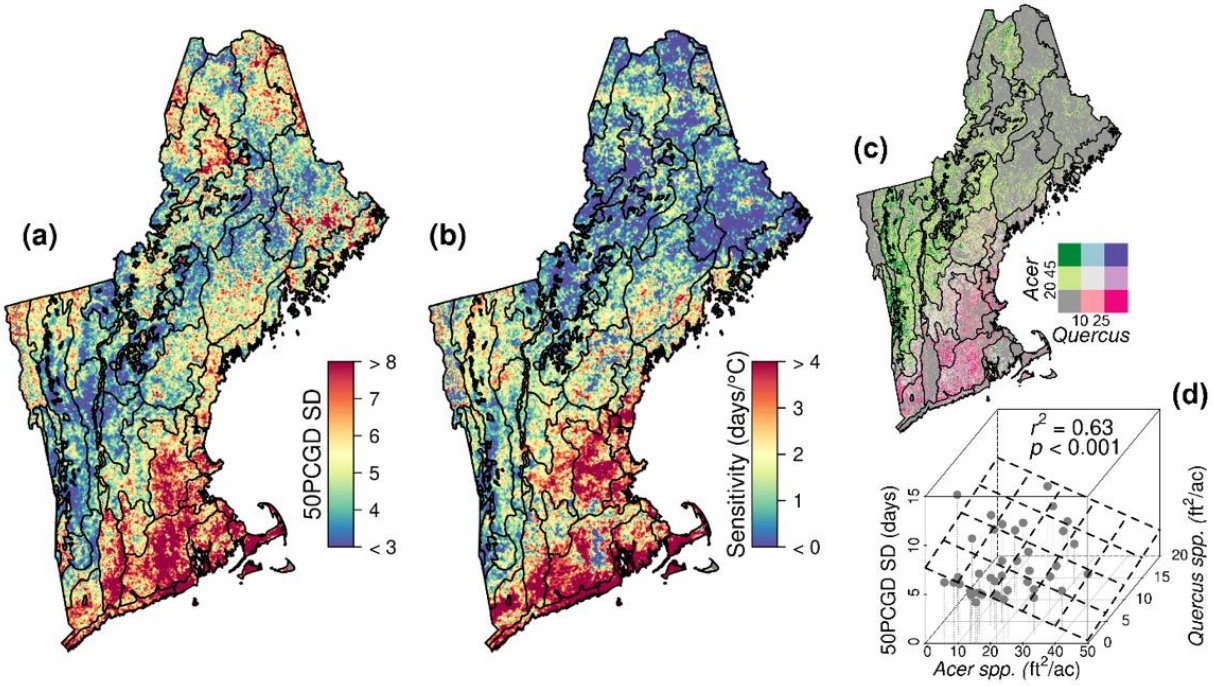

Fig. 5. Geographic variation in (a) the standard deviation (SD) of mid-greendown dates derived from 30 m spatial resolution HLS imagery from 2016-2020, (b) sensitivity to pre-senescence period mean air temperature, and (c) basal area for *Acer* and *Quercus* species. Panel (d) shows results from a multiple linear regression demonstrating that 63% of geographic variation in the magnitude of ecoregion-scale interannual variation in senescence onset dates from remote sensing is explained by the basal area of *Acer* and *Quercus* species in each EPA Level IV ecoregion (n = 40).

4. Discussion

4.1. Bioclimatic controls on leaf senescence

Consistent with previous studies, results from this work support the argument that air temperature and photoperiod are the dominant factors that control the timing of leaf senescence (Archetti et al., 2013; Fracheboud et al., 2009; Gill et al., 2015; Lang et al., 2019; Liu et al., 2020; Vitasse et al., 2021; S. Zhang et al., 2020). However, by quantifying the relative importance among a large suite of bioclimatic controls using a data-driven HBM, we demonstrate that the relative influence of photoperiod and air temperature far exceed the influence of all other bioclimatic controls, and that photoperiod was the most influential control across all 12 deciduous tree species considered in this study. Indeed, excluding photoperiod as a predictor in the HBM substantially degraded the accuracy of model predictions (models M1-M5 versus model M6 in Table 1). Moreover, given the structure of the HBM, which tracks continuous development of leaf senescence at daily time step, our results indicate that the influence of photoperiod on the timing of senescence occurs over an extended period prior to senescence onset. Stated another way, photoperiod exerts continuous forcing that acts in concert with other forcing variables (primarily temperature) and does not simply act as a trigger that initiates senescence after a species-specific threshold is reached. Recent studies using process-based models incorporating a continuous effect of photoperiod (with joint control from air temperature) have reported that these models perform better than process-based models that use photoperiod as a cue (Lang et al., 2019; Liu et al., 2020), which supports our findings.

More generally, by using the HBM to test different sets of bioclimatic controls, results from this study provide useful insights to recent debates regarding the representation of thermal forcing in senescence models (*e.g.*, the role of mean versus minimum versus maximum air temperature)

(Meng et al., 2020; Wu et al., 2018). Specifically, results from the HBM show that daily mean air temperature and the daily range in air temperatures is the most effective combination of thermal forcing variables for predicting the timing of senescence (Table 1), and that larger amplitudes in daily air temperature lead to earlier leaf senescence (Fig. 3c). These results may support the argument that minimum and maximum air temperatures have distinct roles in controlling the timing of leaf senescence (specifically, that higher maximum temperatures lead to earlier leaf senescence, while higher daily minimum temperature lead to later leaf senescence; Wu et al., 2018). However, given that the overall impact of temperature range is relatively modest (as well as the high correlation between daily minimum and maximum temperature), these results should be viewed as a justification for more research rather than definitive evidence.

Significantly, outside of photoperiod and air temperature, none of the forcing variables consistently exerted a substantial influence on the timing of senescence. The dependence of daily temperature range and daily mean VPD was statistically different from zero (*i.e.*, more than 95% of the sampled model coefficients excluded zero; Fig. 3) for only three species in each case (ACPE, BEAL, BEPA and ACPE, BELA, QUVE, respectively), and daily mean PAR was not statistically different from zero for any of the twelve species. Three species (AMAF, BEAL, and PRSE) exhibited negative dependence on the timing of budburst (*i.e.*, earlier budburst leads to earlier senescence) and five species (ACSA, AMAF, BEPA, FRAM, and QUAL) exhibited dependence on early season GPP, with the first four of these species exhibiting positive coefficients (*i.e.*, higher early season GPP leading to earlier leaf senescence). But, for all these latter cases, the magnitude of dependence was small. Hence, outside of photoperiod and daily mean air temperature, the sensitivity of leaf senescence to other bioclimatic forcing variables was either non-significant, or very modest and species-specific. In this context, results from the HBM do not support results

412 from recent studies reporting that early-season GPP (Zani et al., 2020), springtime phenology
413 (Keenan and Richardson, 2015), and VPD (Peng et al., 2021) are important controls on the timing
414 of leaf senescence.

415

416 *4.2. Implications for land surface models*

417 Phenology exerts first-order control on a wide array of ecological functions (*e.g.*,
418 photosynthesis and transpiration) and surface properties (*e.g.*, albedo) that strongly influence water,
419 energy, and carbon exchange in land surface models (Moon et al., 2020; Piao et al., 2019; Xu et
420 al., 2020; Young et al., 2021). Despite this, current models include only very crude (and as a result
421 unrealistic) representation of fall phenology (Richardson et al., 2012). Most land surface models
422 (LSMs) use air, soil, or surface temperature as a primary driver, in conjunction with secondary
423 variables such as day-length (*i.e.*, photoperiod), soil moisture, precipitation, and/or carbon balance,
424 to simulate the timing of leaf senescence (Peano et al., 2021; Richardson et al., 2012). However,
425 results from this study indicate that photoperiod is uniformly the strongest factor controlling the
426 timing of leaf senescence, at least in temperate deciduous forests (Figs. 3 and 4). This mis-
427 parameterization almost certainly explains why current LSMs simulate the timing of senescence
428 so poorly. Moreover, the lower predictive power of the CSM compared to the HBM, especially in
429 capturing interannual variation in the timing of leaf senescence (Fig. 2), implies that current
430 process-based leaf senescence models do not realistically represent the nature and timing of leaf
431 senescence processes. Given this, results from this work suggest that integration of data-driven
432 phenology models, which are able to accurately represent the role of photoperiod, is a promising
433 approach for triggering leaf senescence in the next generation of LSMs that has the potential to

substantially benefit simulations of water, energy and carbon fluxes in these models (Reichstein et al., 2019).

A related conclusion, which also has substantial implications for representation of phenology in LSMs, is that even though all the trees at Harvard Forest experienced the same bioclimatic forcing and changes therein (*i.e.*, warming over the last 30 years (Fig. S3)), individual species responded differently from one another. Specifically, we showed that species-specific dependence on bioclimatic controls among the 12 species examined resulted in divergent responses to climate change over nearly three decades (Fig. 1). Further, using regional-scale land surface phenology data along with stand-level species composition maps, we demonstrated that results obtained at Harvard Forest (*i.e.*, that interannual variation and sensitivity to temperature and photoperiod in the timing of leaf senescence are species-specific characteristics (Fig. 5)) were robust at regional scale. Given that most LSMs classify vegetation into plant functional types and then parameterize phenology sub-models according to plant functional type, our study suggests that this approach may introduce a substantial source of model error in LSM simulation results. Hence, integrating data-driven phenology sub-models and embracing species composition maps using finer spatial satellite imagery such as HLS and perhaps PlanetScope (*c.f.*, Hemmerling et al., 2021; Moon et al., 2021a) may provide a useful basis for improving LSM representation of fall phenology, and by extension, LSM-based simulation of water, carbon and energy exchange.

5. Conclusions

In this study, we assessed how interannual variability in bioclimatic controls affects the timing of leaf senescence in temperate deciduous forests. To do this, we used a data-driven hierarchical

Bayesian model calibrated to nearly three decades of species-specific field measurements of leaf coloration dates for 12 temperate deciduous tree species in New England. To expand and test the generality of our results, we used land surface phenology time series at 30 m spatial resolution derived from remote sensing in combination with species composition maps to show that results obtained at a single site (Harvard Forest) are consistent with the response of senescence to bioclimatic forcing at regional scale. Our results identify three important implications for understanding and modeling the timing of leaf senescence in temperate deciduous forests. First, photoperiod was uniformly more important than air temperature in controlling the timing of leaf senescence in all 12 deciduous tree species that we examined in this study. Second, the data-driven HBM outperformed the more traditional process-based CSM, especially in capturing interannual variation in the timing of leaf senescence, which reinforces the dominant role of photoperiod. Third, phenological responses to long-term trends in air temperatures were species-specific. In particular, species exhibiting stronger photoperiod dependence showed lower inter-annual variation and no trend in the timing of leaf senescence in response to the warming over the last 30 years. In contrast, species showing stronger air temperature dependence showed delayed trends in the timing of senescence that are consistent with a response to warming. Together, these results suggest that accurate forecasting of how the timing of leaf senescence will respond to future climate change requires that models account for how bioclimatic factors control the timing of leaf senescence at the species-level. Data-driven approaches such as the HBM used in this study are promising tools not only for improving models to predict the timing of leaf senescence, but more generally, for improving the representation of phenology in land surface models.

Acknowledgments

This work was supported by NASA grant #80NSSC18K0334 and by NSF award #1702627. Additional funding, through the National Science Foundation's LTER program, supported research at Harvard Forest (DEB-1237491). A.D.R acknowledges support from DEB-1832210 and DEB-1702697.

Author contributions

M.M. and M.A.F designed the analysis and led the drafting of the manuscript. M.M. performed the analysis. A.D.R. contributed analysis ideas and participated in drafting the manuscript. J.O provided the field data.

Competing interests

The authors declare no competing interests.

Supporting Information

Table S1. Species information and acronyms.

Species code	Scientific name	Common name	Number of individual trees used over the study period
ACPE	*Acer pensylvanicum*	Striped maple	4
ACRU	*Acer rubrum*	Red maple	5
ACSA	*Acer saccharum*	Sugar maple	4
AMAF	*Amelanchier alnifolia*	Shadbush	3
BEAL	*Betula alleghaniensis*	Yellow birch	3
BELE	*Betula lenta*	Black birch	3
BEPA	*Betula papyrifera*	Paper birch	8
FRAM	*Fraxinus americana*	White ash	8
PRSE	*Prunus serotina*	Black cherry	4
QUAL	*Quercus alba*	White oak	5
QURU	*Quercus rubra*	Red oak	4
QUVE	*Quercus velutina*	Black oak	6

Table S2. Number of individual observations for each species in each year.

Year \ Species	ACPE	ACRU	ACSA	AMAF	BEAL	BELE	BEPA	FRAM	PRSE	QUAL	QURU	QUVE
1992	3	5	1	3	3	3	1	5	2	2	-	1
1993	4	5	3	3	3	3	4	5	3	3	4	4
1994	4	5	3	3	3	3	4	5	3	3	4	4
1995	4	5	3	3	3	3	4	4	3	3	4	4
1996	4	5	3	3	3	3	4	4	3	3	4	4
1997	4	5	3	3	3	3	4	4	3	3	4	4
1998	4	5	3	3	3	3	4	4	3	3	4	4
1999	4	5	3	3	3	3	4	4	3	3	4	4
2000	4	5	3	3	3	3	4	4	3	3	4	4
2001	4	5	3	3	3	3	4	4	3	3	4	4
2002	4	5	3	3	3	3	4	4	3	3	4	4
2003	4	5	3	3	3	3	4	4	3	3	4	4
2004	4	5	3	3	3	3	4	4	3	3	4	4
2005	4	5	3	3	3	3	4	4	3	3	4	4
2006	4	5	3	3	3	3	4	4	3	3	4	4
2007	4	5	2	3	3	3	4	3	3	3	4	4
2008	4	5	3	3	3	3	4	4	3	3	4	4
2009	4	5	3	3	3	3	4	4	3	3	4	4
2010	4	5	3	3	3	3	4	4	3	3	4	4
2011	4	5	3	3	3	3	4	4	3	3	4	4
2012	4	5	3	3	3	3	3	4	3	3	4	4
2013	4	5	3	3	3	3	4	4	3	3	4	4
2014	4	5	3	3	3	3	4	3	3	3	4	4
2015	4	5	3	3	3	3	4	4	3	3	4	4
2016	4	5	3	3	3	3	3	4	3	3	4	4
2017	4	5	3	3	3	3	3	4	3	3	4	3
2018	4	5	3	3	3	3	4	4	3	3	4	4
2019	4	5	3	3	3	3	4	4	3	3	4	4

Table S3. Process-based model parameters and performance versus HBM.

Species code	CSM Model Parameters						AIC		RMSE	
	a_D	b_D	c_D	P_{crit}	α	γ	HBM	CSM	HBM	CSM
ACPE	1.10	20.31	9.59	12.44	18.75	0.12	73.74	88.18	2.65	3.76
ACRU	1.58	20.65	10.08	12.80	18.16	0.06	72.34	79.45	2.62	3.22
ACSA	0.61	19.61	10.51	12.44	18.78	0.11	94.68	94.82	3.95	4.23
AMAF	0.99	19.95	9.86	12.82	19.06	0.06	81.14	86.20	3.32	3.63
BEAL	0.82	19.65	9.66	12.91	19.46	0.08	62.05	63.66	1.81	2.43
BELE	1.23	20.21	10.01	12.52	18.32	0.10	60.34	70.42	2.22	2.74
BEPA	1.61	20.48	9.84	12.62	18.56	-0.03	106.99	108.42	5.10	5.40
FRAM	0.98	20.05	9.90	12.95	19.34	0.01	88.72	100.64	3.58	4.70
PRSE	0.81	20.02	9.92	12.29	19.52	0.22	70.26	78.77	2.62	3.18
QUAL	1.19	19.97	9.86	12.44	18.77	0.22	72.77	91.06	2.85	3.96
QURU	0.81	20.84	9.81	11.94	19.25	0.01	68.46	81.51	2.37	3.49
QUVE	0.95	20.09	9.71	12.31	19.55	0.13	69.15	86.20	2.54	3.63
Average	1.06	20.15	9.90	12.54	18.96	0.09	76.72	85.78	2.97	3.70

CSM: Caffarra's model; HBM: Hierarchical Bayesian model; P_{crit} is a threshold for day-length; α and γ are parameters regulating the effects of changes in spring leaf unfolding date on leaf senescence date; AIC: Akaike information criterion.

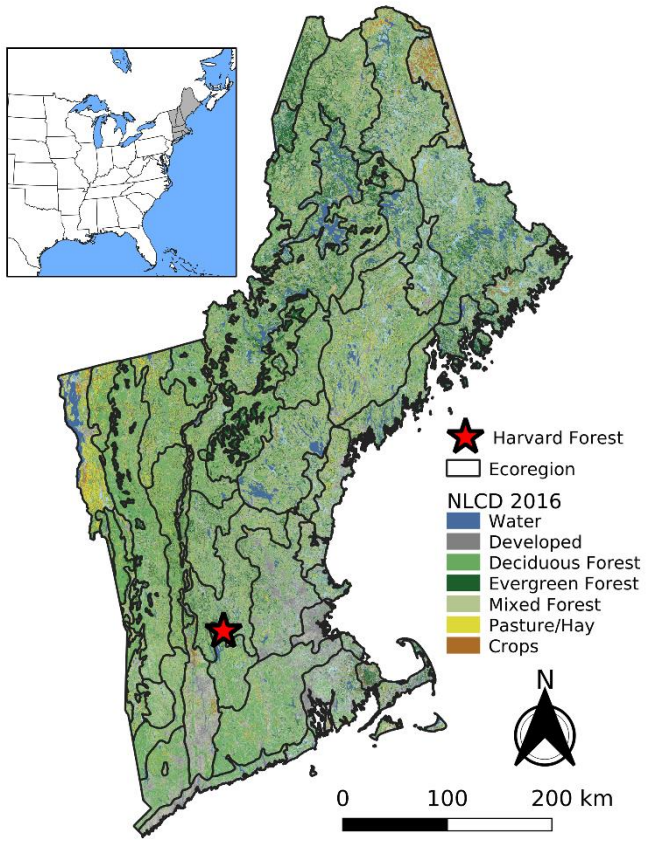

Fig. S1. Map of the study area showing the location of Harvard Forest. Black polygons show the Level IV EPA ecoregions and the background is land cover from the USGS National Land Cover Database (USGS and Rigge, 2019) in 2016.

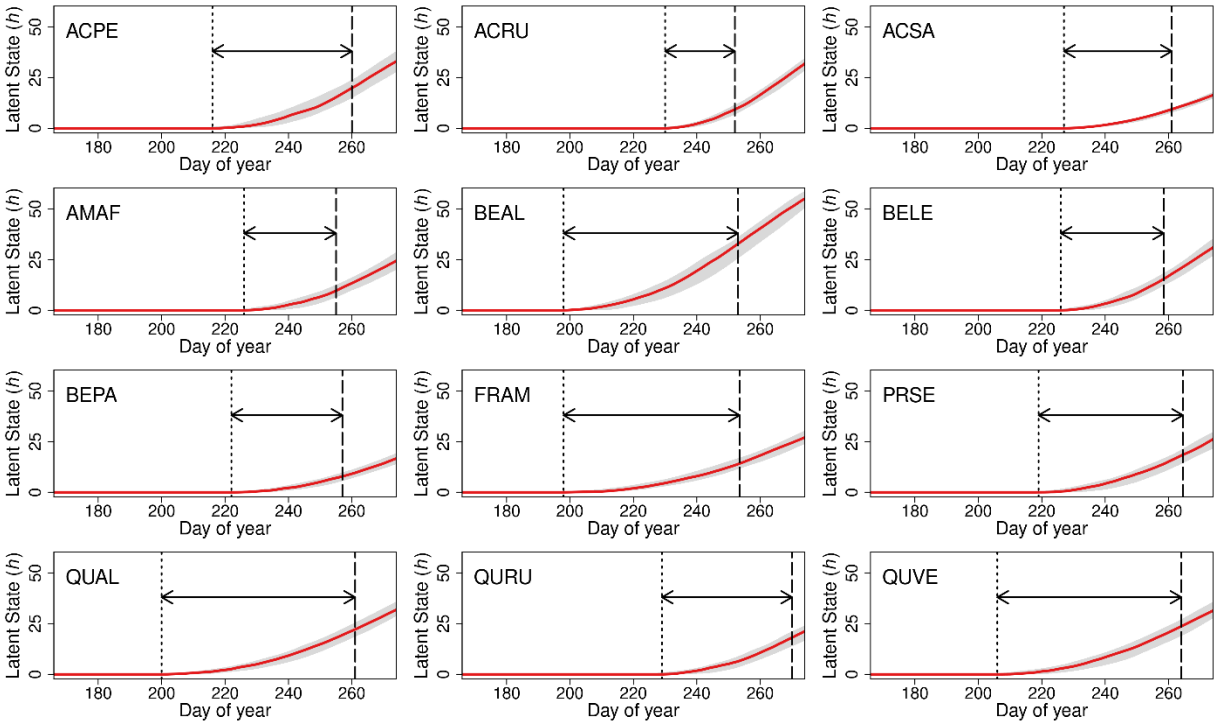

513

514 **Fig. S2.** Solid red lines and shaded areas represent the mean and standard deviation in time series
515 of the latent state across 28 years, respectively. The horizontal arrows identify the time period
516 when phenological development (*i.e.*, leaf senescence) is affected by bioclimatic forcing, which
517 ranges from 21 to 61 days with the mean of 42 days across the species.

518

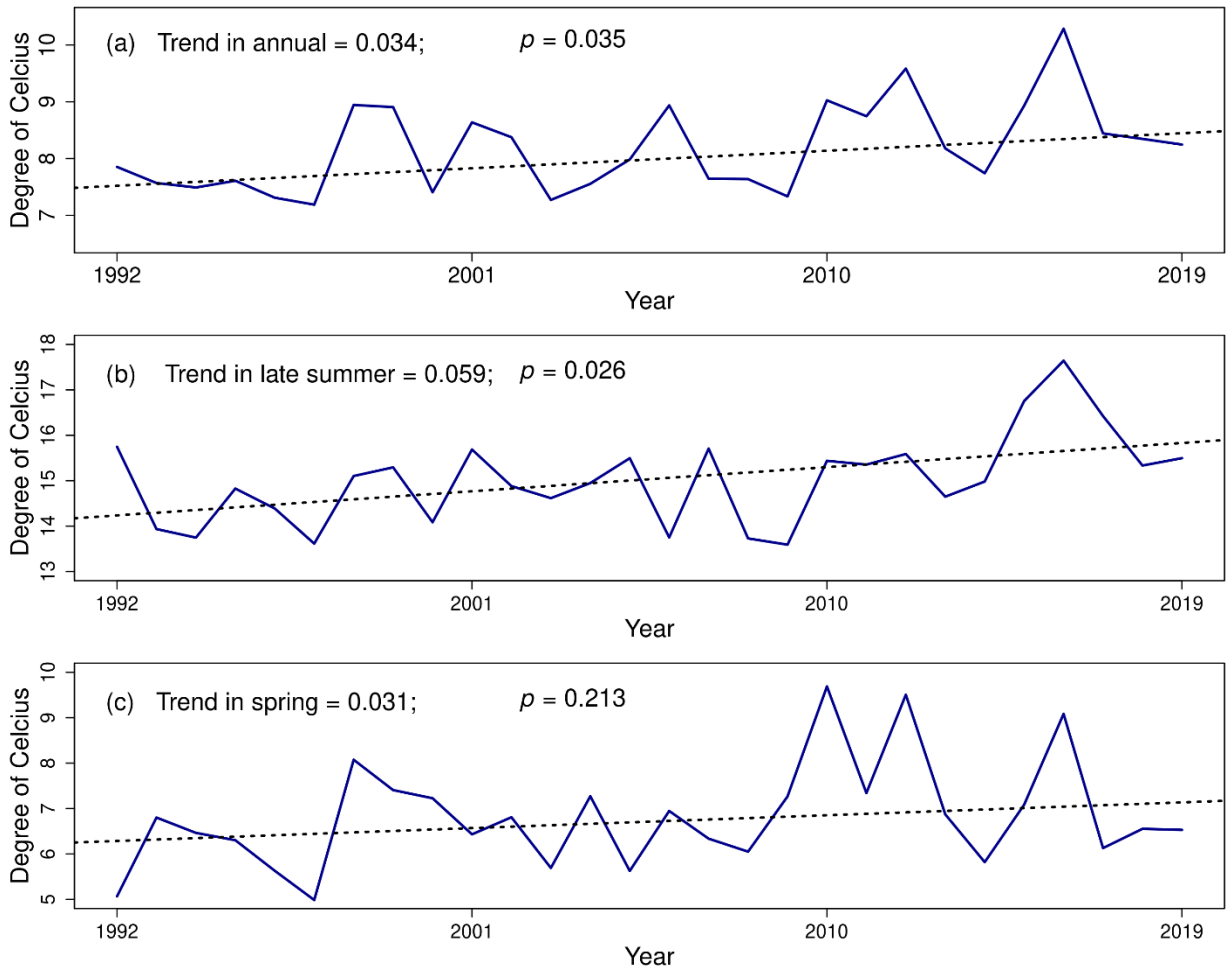

519

520 **Fig. S3.** Air temperature at Harvard Forest for (a) annual, (b) late summer (from August to
521 October), and (c) spring (from March to May). Dotted lines show the long-term trend based on
522 Theil-Sen.

523

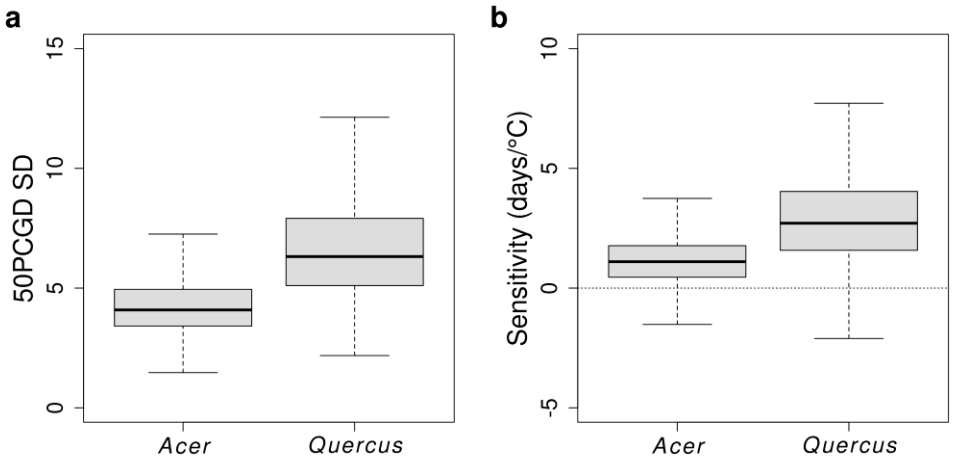

524

525 **Fig. S4**. Boxplots for (a) the standard deviation (SD) of mid-greendown dates (50PCGD) derived
526 from 30 m spatial resolution HLS imagery from 2016-2020 and (b) sensitivity to pre-senescence
527 period mean air temperature. For each panel, '*Acer*' represent distribution for pixels where the
528 basal area for *Acer* species is greater than 20 ft^2/ac and those for *Quercus* species is less than 10
529 ft^2/ac; while '*Quercus*' represent distribution for pixels where the basal area for *Acer* species is
530 less than 20 ft^2/ac and those for *Quercus* species is greater than 10 ft^2/ac.

531

References

Archetti, M., Richardson, A.D., O'Keefe, J., Delpierre, N., 2013. Predicting Climate Change Impacts on the Amount and Duration of Autumn Colors in a New England Forest. PLoS ONE 8, e57373. https://doi.org/10.1371/journal.pone.0057373

Bigler, C., Vitasse, Y., 2021. Premature leaf discoloration of European deciduous trees is caused by drought and heat in late spring and cold spells in early fall. Agricultural and Forest Meteorology 307, 108492. https://doi.org/10.1016/j.agrformet.2021.108492

Bonan, G.B., 2008. Forests and Climate Change: Forcings, Feedbacks, and the Climate Benefits of Forests. Science 320, 1444–1449. https://doi.org/10.1126/science.1155121

Buermann, W., Forkel, M., O'Sullivan, M., Sitch, S., Friedlingstein, P., Haverd, V., Jain, A.K., Kato, E., Kautz, M., Lienert, S., Lombardozzi, D., Nabel, J.E.M.S., Tian, H., Wiltshire, A.J., Zhu, D., Smith, W.K., Richardson, A.D., 2018. Widespread seasonal compensation effects of spring warming on northern plant productivity. Nature 562, 110–114. https://doi.org/10.1038/s41586-018-0555-7

Caffarra, A., Donnelly, A., Chuine, I., 2011. Modelling the timing of Betula pubescens budburst. II. Integrating complex effects of photoperiod into process-based models. Clim. Res. 46, 159–170. https://doi.org/10.3354/cr00983

Chen, L., Hänninen, H., Rossi, S., Smith, N.G., Pau, S., Liu, Z., Feng, G., Gao, J., Liu, J., 2020. Leaf senescence exhibits stronger climatic responses during warm than during cold autumns. Nature Climate Change 1–4. https://doi.org/10.1038/s41558-020-0820-2

Clark, J.S., Melillo, J., Mohan, J., Salk, C., 2014a. The seasonal timing of warming that controls onset of the growing season. Global Change Biology 20, 1136–1145. https://doi.org/10.1111/gcb.12420

Clark, J.S., Salk, C., Melillo, J., Mohan, J., 2014b. Tree phenology responses to winter chilling, spring warming, at north and south range limits. Functional Ecology 28, 1344–1355. https://doi.org/10.1111/1365-2435.12309

Claverie, M., Ju, J., Masek, J.G., Dungan, J.L., Vermote, E.F., Roger, J.-C., Skakun, S.V., Justice, C., 2018. The Harmonized Landsat and Sentinel-2 surface reflectance data set. Remote Sensing of Environment 219, 145–161. https://doi.org/10.1016/j.rse.2018.09.002

Delpierre, N., Dufrêne, E., Soudani, K., Ulrich, E., Cecchini, S., Boé, J., François, C., 2009. Modelling interannual and spatial variability of leaf senescence for three deciduous tree species in France. Agricultural and Forest Meteorology 149, 938–948. https://doi.org/10.1016/j.agrformet.2008.11.014

Delpierre, N., Vitasse, Y., Chuine, I., Guillemot, J., Bazot, S., Rutishauser, T., Rathgeber, C.B.K., 2016. Temperate and boreal forest tree phenology: from organ-scale processes to terrestrial ecosystem models. Annals of Forest Science 73, 5–25. https://doi.org/10.1007/s13595-015-0477-6

Dox, I., Gričar, J., Marchand, L.J., Leys, S., Zuccarini, P., Geron, C., Prislan, P., Mariën, B., Fonti, P., Lange, H., Peñuelas, J., Van den Bulcke, J., Campioli, M., 2020. Timeline of autumn phenology in temperate deciduous trees. Tree Physiology 40, 1001–1013. https://doi.org/10.1093/treephys/tpaa058

Dunn, R.J.H., Aldred, F., Gobron, N., Miller, J.B., Willett, K.M., Ades, M., Adler, R., Richard, P.A., Allan, R., Anderson, J., Argüez, A., Arosio, C., Augustine, J.A., Azorin-Molina, C., Barichivich, J., Beck, H.E., Becker, A., Bellouin, N., Benedetti, A., Berry, D.I., Blenkinsop, S., Bock, O., Bodin, X., Bosilovich, M.G., Boucher, O., Buehler, S.A., Calmettes, B., Carrea, L., Castia, L., Christiansen, H.H., Christy, J.R., Chung, E.-S., Coldewey-Egbers, M., Cooper, O.R., Cornes, R.C., Covey, C., Cretaux, J.-F., Crotwell, M., Davis, S.M., Jeu, R.A.M. de, Degenstein, D., Delaloye, R., Girolamo, L.D., Donat, M.G., Dorigo, W.A., Durre, I., Dutton, G.S., Duveiller, G., Elkins, J.W., Fioletov, V.E., Flemming, J., Foster, M.J., Frith, S.M., Froidevaux, L., Garforth, J.,

Gentry, M., Gupta, S.K., Hahn, S., Haimberger, L., Hall, B.D., Harris, I., Hemming, D.L., Hirschi, M., Ho, S. (Ben), Hrbacek, F., Hubert, D., Hurst, D.F., Inness, A., Isaksen, K., John, V.O., Jones, P.D., Junod, R., Kaiser, J.W., Kaufmann, V., Kellerer-Pirklbauer, A., Kent, E.C., Kidd, R., Kim, H., Kipling, Z., Koppa, A., Kraemer, B.M., Kratz, D.P., Lan, X., Lantz, K.O., Lavers, D., Loeb, N.G., Loyola, D., Madelon, R., Mayer, M., McCabe, M.F., McVicar, T.R., Mears, C.A., Merchant, C.J., Miralles, D.G., Moesinger, L., Montzka, S.A., Morice, C., Mösinger, L., Mühle, J., Nicolas, J.P., Noetzli, J., Noll, B., O'Keefe, J., Osborn, T.J., Park, T., Pasik, A.J., Pellet, C., Pelto, M.S., Perkins-Kirkpatrick, S.E., Petron, G., Phillips, C., Po-Chedley, S., Polvani, L., Preimesberger, W., Rains, D.G., Randel, W.J., Rayner, N.A., Rémy, S., Ricciardulli, L., Richardson, A.D., Robinson, D.A., Rodell, M., Rodríguez-Fernández, N.J., Rosenlof, K.H., Roth, C., Rozanov, A., Rutishäuser, T., Sánchez-Lugo, A., Sawaengphokhai, P., Scanlon, T., Schenzinger, V., Schlegel, R.W., Sharma, S., Shi, L., Simmons, A.J., Siso, C., Smith, S.L., Soden, B.J., Sofieva, V., Sparks, T.H., Stackhouse, P.W., Steinbrecht, W., Stengel, M., Streletskiy, D.A., Sun-Mack, S., Tans, P., Thackeray, S.J., Thibert, E., Tokuda, D., Tourpali, K., Tye, M.R., A, R. van der, Schalie, R. van der, Schrier, G. van der, Vliet, M. van der, Werf, G.R. van der, Vance, A., Vernier, J.-P., Vimont, I.J., Vömel, H., Vose, R.S., Wang, R., Weber, M., Wiese, D., Wilber, A.C., Wild, J.D., Wong, T., Woolway, R.I., Zhou, X., Yin, X., Zhao, G., Zhao, L., Ziemke, J.R., Ziese, M., Zotta, R.M., 2021. Global Climate. Bulletin of the American Meteorological Society 102, S11–S142. https://doi.org/10.1175/BAMS-D-21-0098.1

Estiarte, M., Peñuelas, J., 2015. Alteration of the phenology of leaf senescence and fall in winter deciduous species by climate change: effects on nutrient proficiency. Global Change Biology 21, 1005–1017. https://doi.org/10.1111/gcb.12804

Fracheboud, Y., Luquez, V., Björkén, L., Sjödin, A., Tuominen, H., Jansson, S., 2009. The Control of Autumn Senescence in European Aspen. Plant Physiology 149, 1982–1991. https://doi.org/10.1104/pp.108.133249

Friedl, M.A., 2021. MuSLI Multi-Source Land Surface Phenology Yearly North America 30 m V011. distributed by NASA EOSDIS Land Processes DAAC. https://doi.org/10.5067/Community/MuSLI/MSLSP30NA.011

Friedman, J.M., Roelle, J.E., Cade, B.S., 2011. Genetic and environmental influences on leaf phenology and cold hardiness of native and introduced riparian trees. Int J Biometeorol 55, 775–787. https://doi.org/10.1007/s00484-011-0494-6

Fu, Y.H., Piao, S., Delpierre, N., Hao, F., Hänninen, H., Liu, Y., Sun, W., Janssens, I.A., Campioli, M., 2018. Larger temperature response of autumn leaf senescence than spring leaf-out phenology. Global Change Biology 24, 2159–2168. https://doi.org/10.1111/gcb.14021

Gallinat, A.S., Primack, R.B., Wagner, D.L., 2015. Autumn, the neglected season in climate change research. Trends in Ecology & Evolution 30, 169–176. https://doi.org/10.1016/j.tree.2015.01.004

Gao, F., Anderson, M.C., Zhang, X., Yang, Z., Alfieri, J.G., Kustas, W.P., Mueller, R., Johnson, D.M., Prueger, J.H., 2017. Toward mapping crop progress at field scales through fusion of Landsat and MODIS imagery. Remote Sensing of Environment 188, 9–25. https://doi.org/10.1016/j.rse.2016.11.004

Gill, A.L., Gallinat, A.S., Sanders-DeMott, R., Rigden, A.J., Short Gianotti, D.J., Mantooth, J.A., Templer, P.H., 2015. Changes in autumn senescence in northern hemisphere deciduous trees: a meta-analysis of autumn phenology studies. Ann Bot 116, 875–888. https://doi.org/10.1093/aob/mcv055

Hänninen, H., Kramer, K., Tanino, K., Zhang, R., Wu, J., Fu, Y.H., 2019. Experiments Are Necessary in Process-Based Tree Phenology Modelling. Trends in Plant Science 24, 199–209. https://doi.org/10.1016/j.tplants.2018.11.006

Havé, M., Marmagne, A., Chardon, F., Masclaux-Daubresse, C., 2017. Nitrogen remobilization during leaf senescence: lessons from Arabidopsis to crops. Journal of Experimental Botany 68, 2513–2529. https://doi.org/10.1093/jxb/erw365

Hemmerling, J., Pflugmacher, D., Hostert, P., 2021. Mapping temperate forest tree species using dense Sentinel-2 time series. Remote Sensing of Environment 267, 112743. https://doi.org/10.1016/j.rse.2021.112743

Jiang, Z., Huete, A.R., Didan, K., Miura, T., 2008. Development of a two-band enhanced vegetation index without a blue band. Remote Sensing of Environment 112, 3833–3845. https://doi.org/10.1016/j.rse.2008.06.006

Keenan, T.F., Darby, B., Felts, E., Sonnentag, O., Friedl, M.A., Hufkens, K., O'Keefe, J., Klosterman, S., Munger, J.W., Toomey, M., Richardson, A.D., 2014. Tracking forest phenology and seasonal physiology using digital repeat photography: a critical assessment. Ecological Applications 24, 1478–1489. https://doi.org/10.1890/13-0652.1

Keenan, T.F., Richardson, A.D., 2015. The timing of autumn senescence is affected by the timing of spring phenology: implications for predictive models. Global Change Biology 21, 2634–2641. https://doi.org/10.1111/gcb.12890

Keskitalo, J., Bergquist, G., Gardeström, P., Jansson, S., 2005. A Cellular Timetable of Autumn Senescence. Plant Physiology 139, 1635–1648. https://doi.org/10.1104/pp.105.066845

Lang, W., Chen, X., Qian, S., Liu, G., Piao, S., 2019. A new process-based model for predicting autumn phenology: How is leaf senescence controlled by photoperiod and temperature coupling? Agricultural and Forest Meteorology 268, 124–135. https://doi.org/10.1016/j.agrformet.2019.01.006

Leuzinger, S., Luo, Y., Beier, C., Dieleman, W., Vicca, S., Körner, C., 2011. Do global change experiments overestimate impacts on terrestrial ecosystems? Trends in Ecology & Evolution 26, 236–241. https://doi.org/10.1016/j.tree.2011.02.011

Liu, Q., Piao, S., Campioli, M., Gao, M., Fu, Y.H., Wang, K., He, Y., Li, X., Janssens, I.A., 2020. Modeling leaf senescence of deciduous tree species in Europe. Global Change Biology 26, 4104–4118. https://doi.org/10.1111/gcb.15132

Mann, H.B., 1945. Nonparametric Tests Against Trend. Econometrica 13, 245–259. https://doi.org/10.2307/1907187

Meng, L., Zhou, Y., Li, X., Asrar, G.R., Mao, J., Wanamaker, A.D., Wang, Y., 2020. Divergent responses of spring phenology to daytime and nighttime warming. Agricultural and Forest Meteorology 281, 107832. https://doi.org/10.1016/j.agrformet.2019.107832

Moon, M., Li, D., Liao, W., Rigden, A.J., Friedl, M.A., 2020. Modification of surface energy balance during springtime: The relative importance of biophysical and meteorological changes. Agricultural and Forest Meteorology 284, 107905. https://doi.org/10.1016/j.agrformet.2020.107905

Moon, M., Richardson, A.D., Friedl, M.A., 2021a. Multiscale assessment of land surface phenology from harmonized Landsat 8 and Sentinel-2, PlanetScope, and PhenoCam imagery. Remote Sensing of Environment 266, 112716. https://doi.org/10.1016/j.rse.2021.112716

Moon, M., Seyednasrollah, B., Richardson, A.D., Friedl, M.A., 2021b. Using time series of MODIS land surface phenology to model temperature and photoperiod controls on spring greenup in North American deciduous forests. Remote Sensing of Environment 260, 112466. https://doi.org/10.1016/j.rse.2021.112466

Munger, W., Wofsy, S., 2020. Canopy-Atmosphere Exchange of Carbon, Water and Energy at Harvard Forest EMS Tower since 1991. Harvard Forest Data Archive: HF004 (v.32). https://doi.org/10.6073/pasta/6e1e3d902387781c1d9822cce8444ede

Nelder, J.A., Mead, R., 1965. A Simplex Method for Function Minimization. The Computer Journal 7, 308–313. https://doi.org/10.1093/comjnl/7.4.308

O'Keefe, J., 2019. Phenology of Woody Species at Harvard Forest since 1990. Harvard Forest Data Archive: HF003. https://doi.org/10.6073/pasta/91e3b7c2548a0f2e251729eeacbce312

Park, T., Ganguly, S., Tømmervik, H., Euskirchen, E.S., Høgda, K.-A., Karlsen, S.R., Brovkin, V., Nemani, R.R., Myneni, R.B., 2016. Changes in growing season duration and productivity of

680 northern vegetation inferred from long-term remote sensing data. Environ. Res. Lett. 11, 084001.
681 https://doi.org/10.1088/1748-9326/11/8/084001
682 Peano, D., Hemming, D., Materia, S., Delire, C., Fan, Y., Joetzjer, E., Lee, H., Nabel, J.E.M.S., Park, T.,
683 Peylin, P., Wårlind, D., Wiltshire, A., Zaehle, S., 2021. Plant phenology evaluation of
684 CRESCENDO land surface models – Part 1: Start and end of the growing season. Biogeosciences
685 18, 2405–2428. https://doi.org/10.5194/bg-18-2405-2021
686 Peng, J., Wu, C., Wang, X., Lu, L., 2021. Spring phenology outweighed climate change in determining
687 autumn phenology on the Tibetan Plateau. International Journal of Climatology 41, 3725–3742.
688 https://doi.org/10.1002/joc.7045
689 Peng, J., Wu, C., Zhang, X., Wang, X., Gonsamo, A., 2019. Satellite detection of cumulative and lagged
690 effects of drought on autumn leaf senescence over the Northern Hemisphere. Global Change
691 Biology 25, 2174–2188. https://doi.org/10.1111/gcb.14627
692 Piao, S., Liu, Q., Chen, A., Janssens, I.A., Fu, Y., Dai, J., Liu, L., Lian, X., Shen, M., Zhu, X., 2019. Plant
693 phenology and global climate change: current progresses and challenges. Global Change Biology.
694 https://doi.org/10.1111/gcb.14619
695 Primack, R.B., Laube, J., Gallinat, A.S., Menzel, A., 2015. From observations to experiments in
696 phenology research: investigating climate change impacts on trees and shrubs using dormant
697 twigs. Annals of Botany 116, 889–897. https://doi.org/10.1093/aob/mcv032
698 Reichstein, M., Camps-Valls, G., Stevens, B., Jung, M., Denzler, J., Carvalhais, N., Prabhat, 2019. Deep
699 learning and process understanding for data-driven Earth system science. Nature 566, 195.
700 https://doi.org/10.1038/s41586-019-0912-1
701 Renner, S.S., Zohner, C.M., 2018. Climate Change and Phenological Mismatch in Trophic Interactions
702 Among Plants, Insects, and Vertebrates. Annu. Rev. Ecol. Evol. Syst. 49, 165–182.
703 https://doi.org/10.1146/annurev-ecolsys-110617-062535
704 Richardson, A.D., Anderson, R.S., Arain, M.A., Barr, A.G., Bohrer, G., Chen, G., Chen, J.M., Ciais, P.,
705 Davis, K.J., Desai, A.R., Dietze, M.C., Dragoni, D., Garrity, S.R., Gough, C.M., Grant, R.,
706 Hollinger, D.Y., Margolis, H.A., McCaughey, H., Migliavacca, M., Monson, R.K., Munger, J.W.,
707 Poulter, B., Raczka, B.M., Ricciuto, D.M., Sahoo, A.K., Schaefer, K., Tian, H., Vargas, R.,
708 Verbeeck, H., Xiao, J., Xue, Y., 2012. Terrestrial biosphere models need better representation of
709 vegetation phenology: results from the North American Carbon Program Site Synthesis. Global
710 Change Biology 18, 566–584. https://doi.org/10.1111/j.1365-2486.2011.02562.x
711 Richardson, A.D., Bailey, A.S., Denny, E.G., Martin, C.W., O'keefe, J., 2006. Phenology of a northern
712 hardwood forest canopy. Global Change Biology 12, 1174–1188. https://doi.org/10.1111/j.1365-
713 2486.2006.01164.x
714 Richardson, A.D., Hufkens, K., Milliman, T., Aubrecht, D.M., Furze, M.E., Seyednasrollah, B.,
715 Krassovski, M.B., Latimer, J.M., Nettles, W.R., Heiderman, R.R., Warren, J.M., Hanson, P.J.,
716 2018. Ecosystem warming extends vegetation activity but heightens vulnerability to cold
717 temperatures. Nature. https://doi.org/10.1038/s41586-018-0399-1
718 Schaber, J., Badeck, F.-W., 2003. Physiology-based phenology models for forest tree species in Germany.
719 Int J Biometeorol 47, 193–201. https://doi.org/10.1007/s00484-003-0171-5
720 Sen, P.K., 1968. Estimates of the Regression Coefficient Based on Kendall's Tau. Journal of the
721 American Statistical Association 63, 1379–1389. https://doi.org/10.2307/2285891
722 Su, Y.-S., Yajima, M., 2015. R2jags: Using R to Run "JAGS". R package version 0.5-7 34.
723 USGS, Rigge, M., 2019. National Land Cover Database (NLCD) 2016 Shrubland Fractional Components
724 for the Western U.S. (ver. 3.0, July 2020): U.S. Geological Survey data release.
725 https://doi.org/10.5066/P9MJVQSQ
726 Vitasse, Y., Baumgarten, F., Zohner, C.M., Kaewthongrach, R., Fu, Y.H., Walde, M.G., Moser, B., 2021.
727 Impact of microclimatic conditions and resource availability on spring and autumn phenology of
728 temperate tree seedlings. New Phytol nph.17606. https://doi.org/10.1111/nph.17606

729 Vitasse, Y., Lenz, A., Hoch, G., Körner, C., 2014. Earlier leaf-out rather than difference in freezing
730 resistance puts juvenile trees at greater risk of damage than adult trees. Journal of Ecology 102,
731 981–988. https://doi.org/10.1111/1365-2745.12251
732 Wilson, B., Lister, A.J., Riemann, R.I., Griffith, D.M., 2013. Live tree species basal area of the
733 contiguous United States (2000-2009). Newtown Square, PA: USDA Forest Service, Rocky
734 Mountain Research Station. https://doi.org/10.2737/RDS-2013-0013
735 Wolkovich, E.M., Cook, B.I., Allen, J.M., Crimmins, T.M., Betancourt, J.L., Travers, S.E., Pau, S.,
736 Regetz, J., Davies, T.J., Kraft, N.J.B., Ault, T.R., Bolmgren, K., Mazer, S.J., McCabe, G.J.,
737 McGill, B.J., Parmesan, C., Salamin, N., Schwartz, M.D., Cleland, E.E., 2012. Warming
738 experiments underpredict plant phenological responses to climate change. Nature 485, 494–497.
739 https://doi.org/10.1038/nature11014
740 Wu, C., Wang, X., Wang, H., Ciais, P., Peñuelas, J., Myneni, R.B., Desai, A.R., Gough, C.M., Gonsamo,
741 A., Black, A.T., Jassal, R.S., Ju, W., Yuan, W., Fu, Y., Shen, M., Li, S., Liu, R., Chen, J.M., Ge,
742 Q., 2018. Contrasting responses of autumn-leaf senescence to daytime and night-time warming.
743 Nature Climate Change 8, 1092. https://doi.org/10.1038/s41558-018-0346-z
744 Xie, Y., Wang, X., Wilson, A.M., Silander, J.A., 2018. Predicting autumn phenology: How deciduous
745 tree species respond to weather stressors. Agricultural and Forest Meteorology 250–251, 127–
746 137. https://doi.org/10.1016/j.agrformet.2017.12.259
747 Xu, X., Riley, W.J., Koven, C.D., Jia, G., Zhang, X., 2020. Earlier leaf-out warms air in the north. Nat.
748 Clim. Chang. 10, 370–375. https://doi.org/10.1038/s41558-020-0713-4
749 Young, A.M., Friedl, M.A., Seyednasrollah, B., Beamesderfer, E., Carrillo, C.M., Li, X., Moon, M.,
750 Arain, M.A., Baldocchi, D.D., Blanken, P.D., Bohrer, G., Burns, S.P., Chu, H., Desai, A.R.,
751 Griffis, T.J., Hollinger, D.Y., Litvak, M.E., Novick, K., Scott, R.L., Suyker, A.E., Verfaillie, J.,
752 Wood, J.D., Richardson, A.D., 2021. Seasonality in aerodynamic resistance across a range of
753 North American ecosystems. Agricultural and Forest Meteorology 310, 108613.
754 https://doi.org/10.1016/j.agrformet.2021.108613
755 Zani, D., Crowther, T.W., Mo, L., Renner, S.S., Zohner, C.M., 2020. Increased growing-season
756 productivity drives earlier autumn leaf senescence in temperate trees. Science 370, 1066–1071.
757 https://doi.org/10.1126/science.abd8911
758 Zhang, S., Dai, J., Ge, Q., 2020. Responses of Autumn Phenology to Climate Change and the
759 Correlations of Plant Hormone Regulation. Sci Rep 10, 9039. https://doi.org/10.1038/s41598-
760 020-65704-8
761 Zhang, Y., Commane, R., Zhou, S., Williams, A.P., Gentine, P., 2020. Light limitation regulates the
762 response of autumn terrestrial carbon uptake to warming. Nature Climate Change 1–5.
763 https://doi.org/10.1038/s41558-020-0806-0
764 Zohner, C.M., Benito, B.M., Svenning, J.-C., Renner, S.S., 2016. Day length unlikely to constrain
765 climate-driven shifts in leaf-out times of northern woody plants. Nature Climate Change 6, 1120–
766 1123. https://doi.org/10.1038/nclimate3138
767

Figure 1

Click here to access/download;Figure;fig1.tif

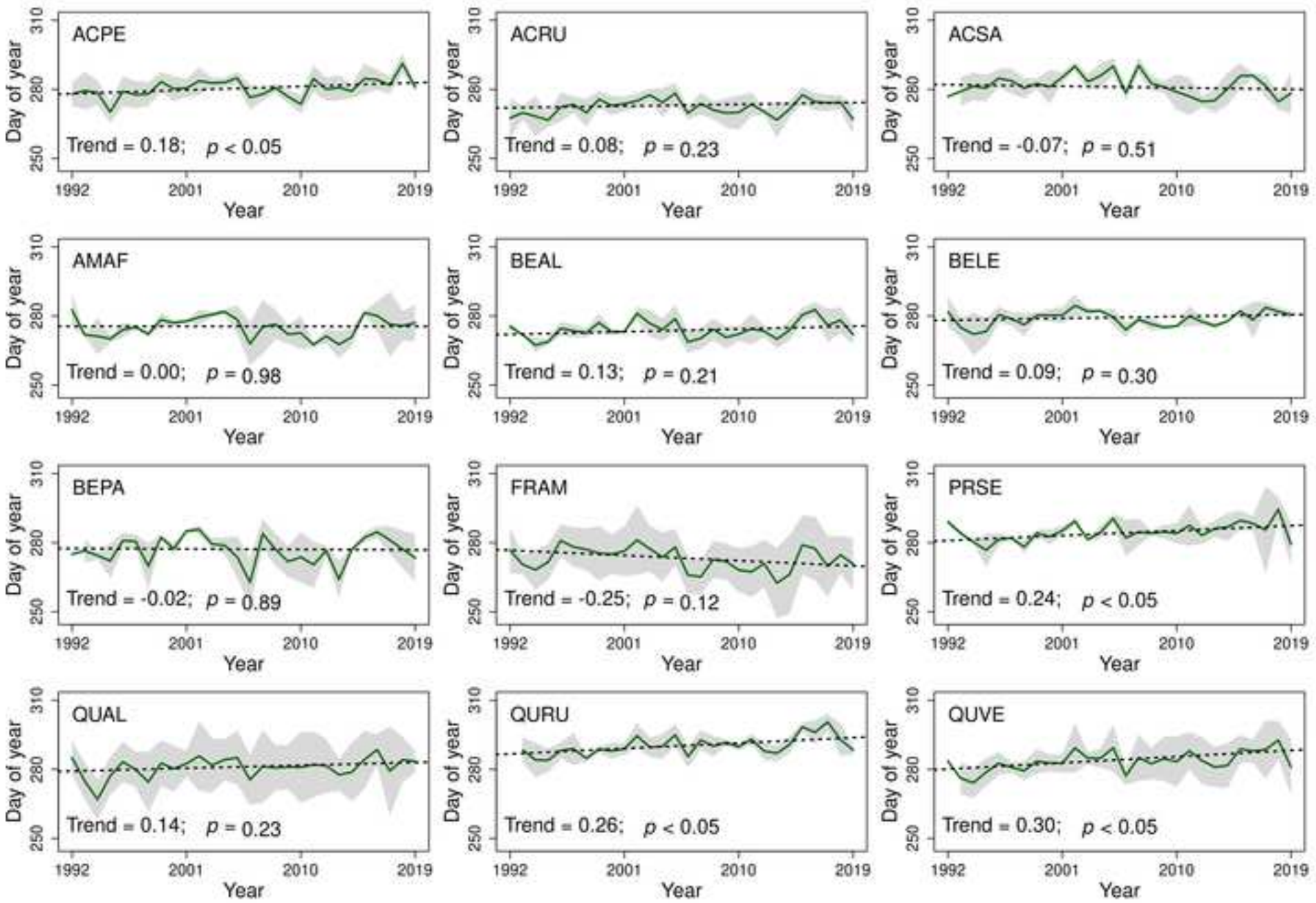

Figure 2

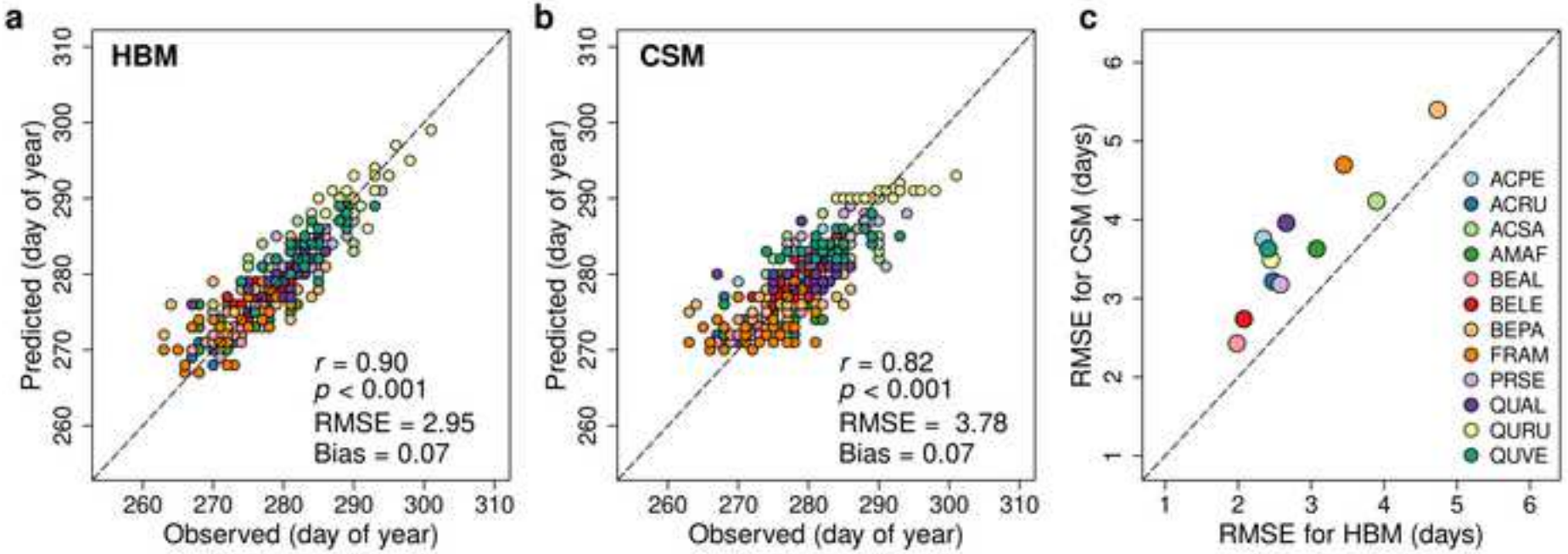

Figure 3

Click here to access/download;Figure;fig3.tif

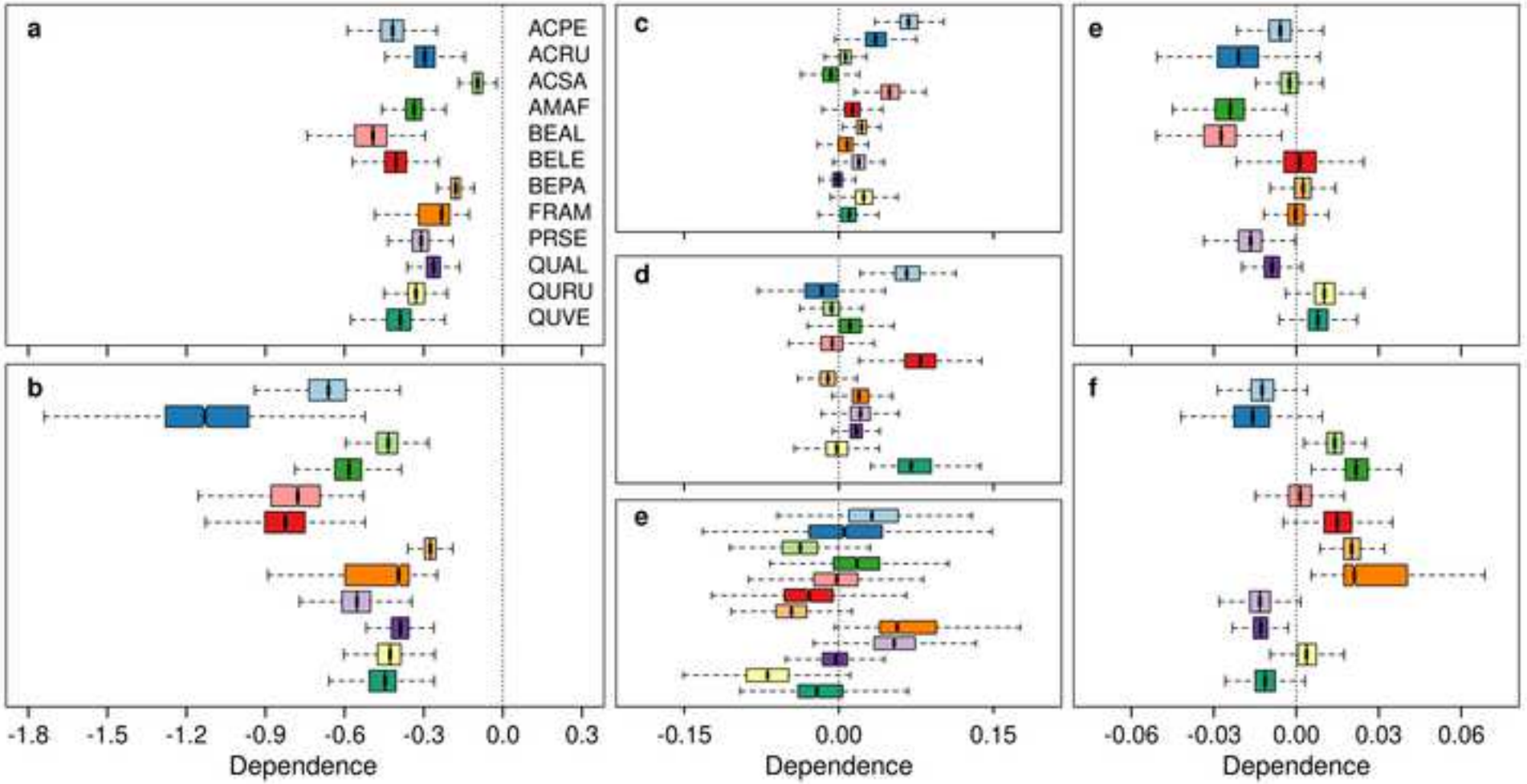

Figure 4

Click here to access/download;Figure;fig4.tif

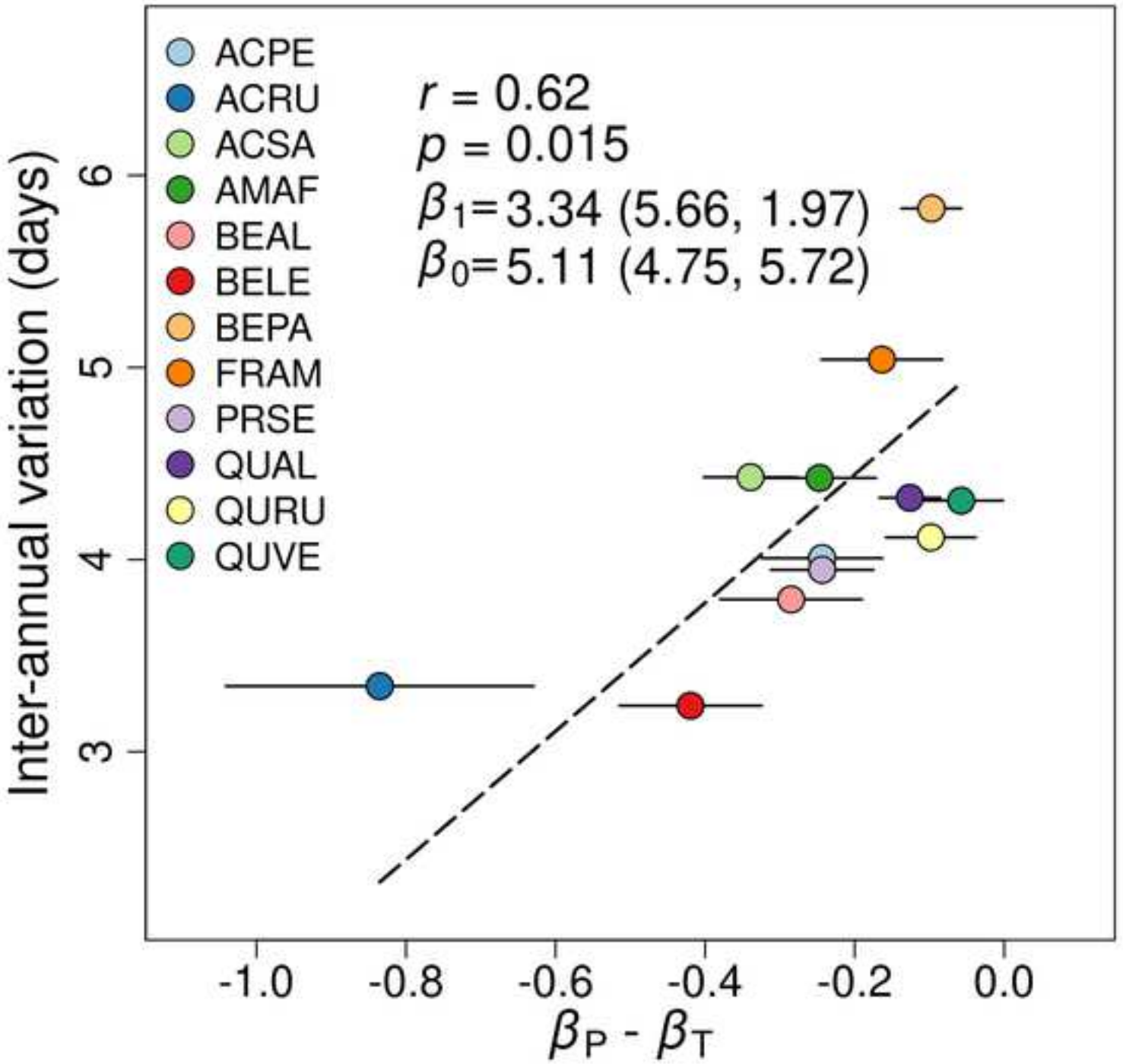

Figure 5

Click here to access/download;Figure;fig5.tif

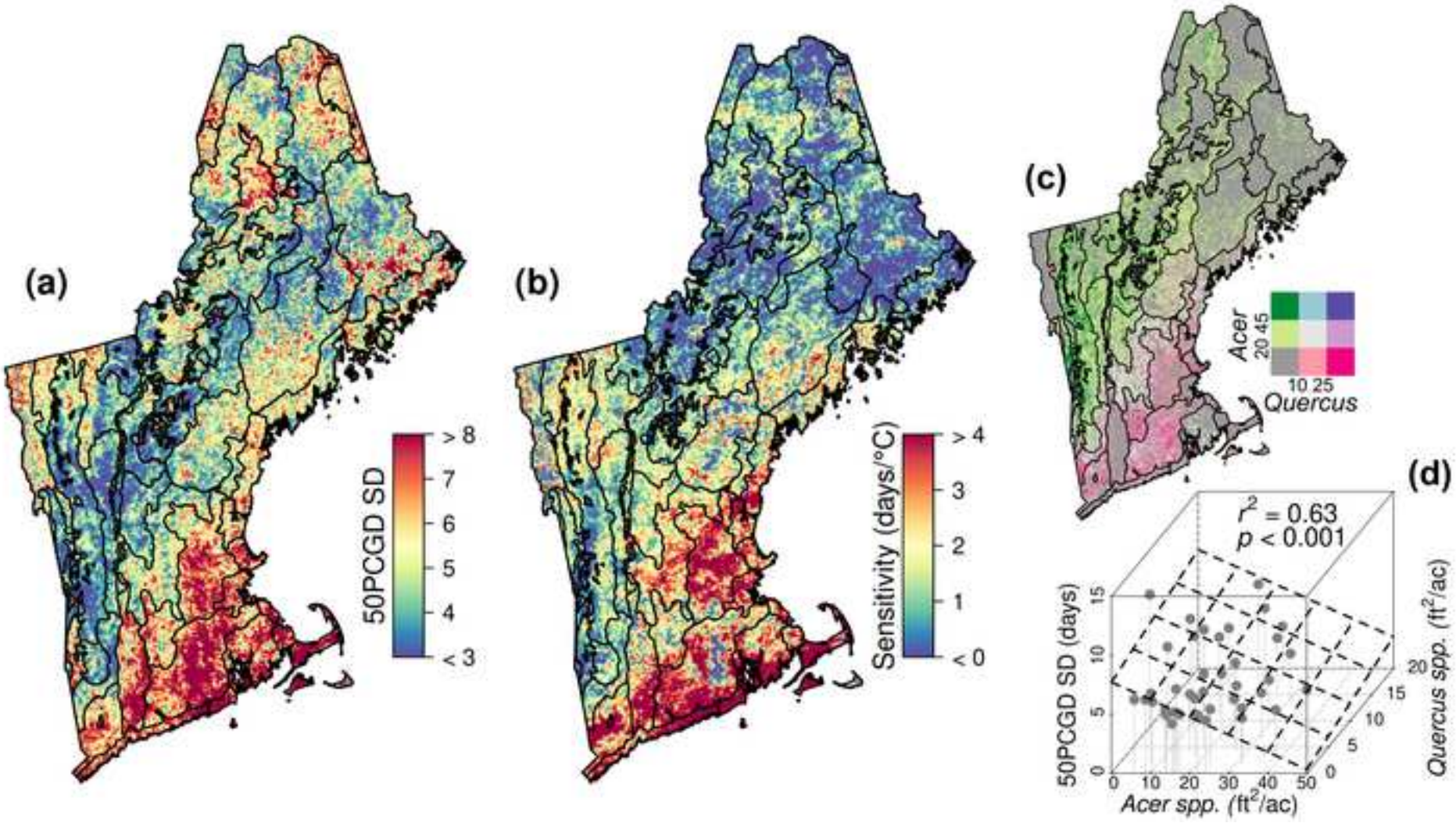

Figure S1

Click here to access/download;Figure;figS1.tif

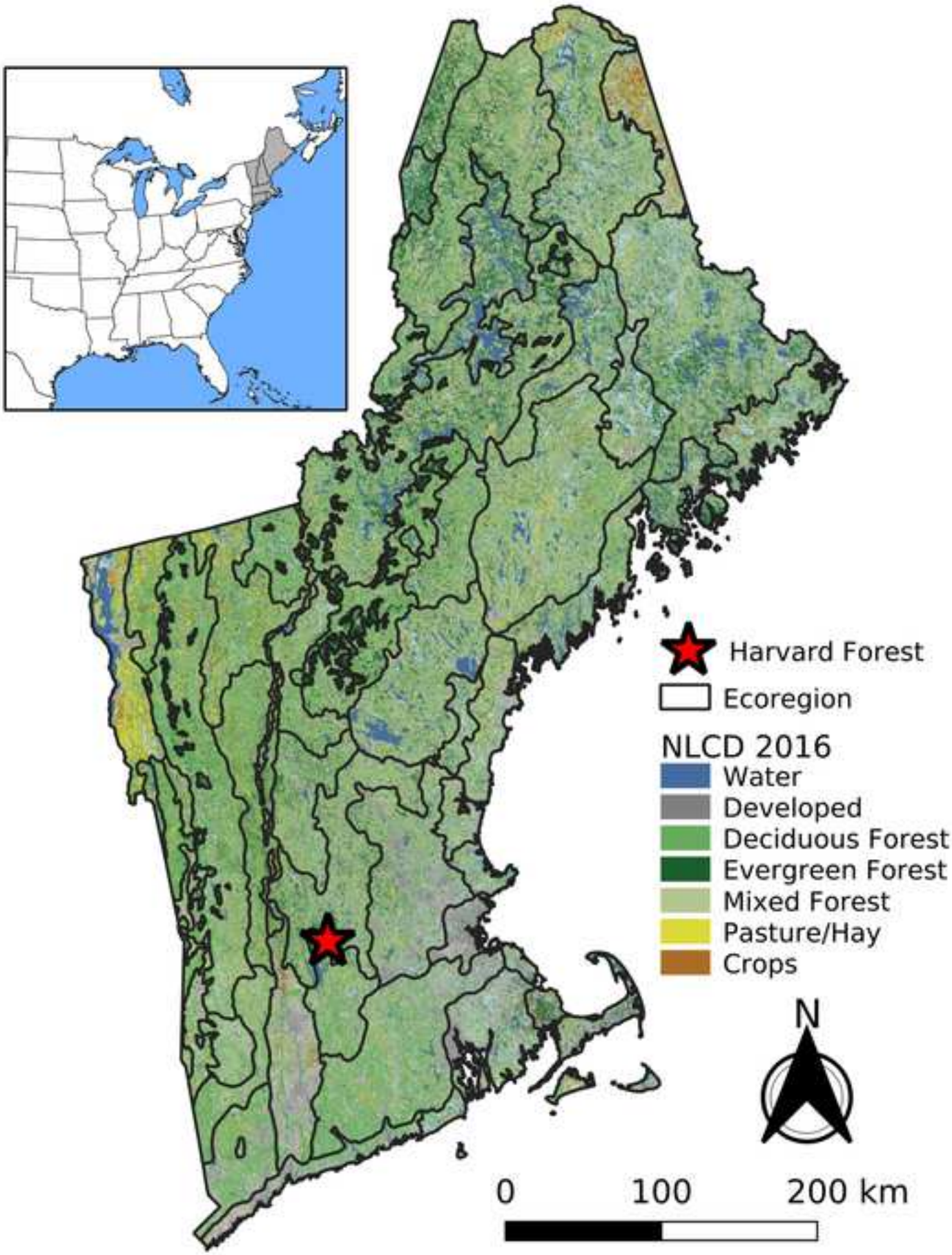

Figure S2

Click here to access/download;Figure;figS2.tif

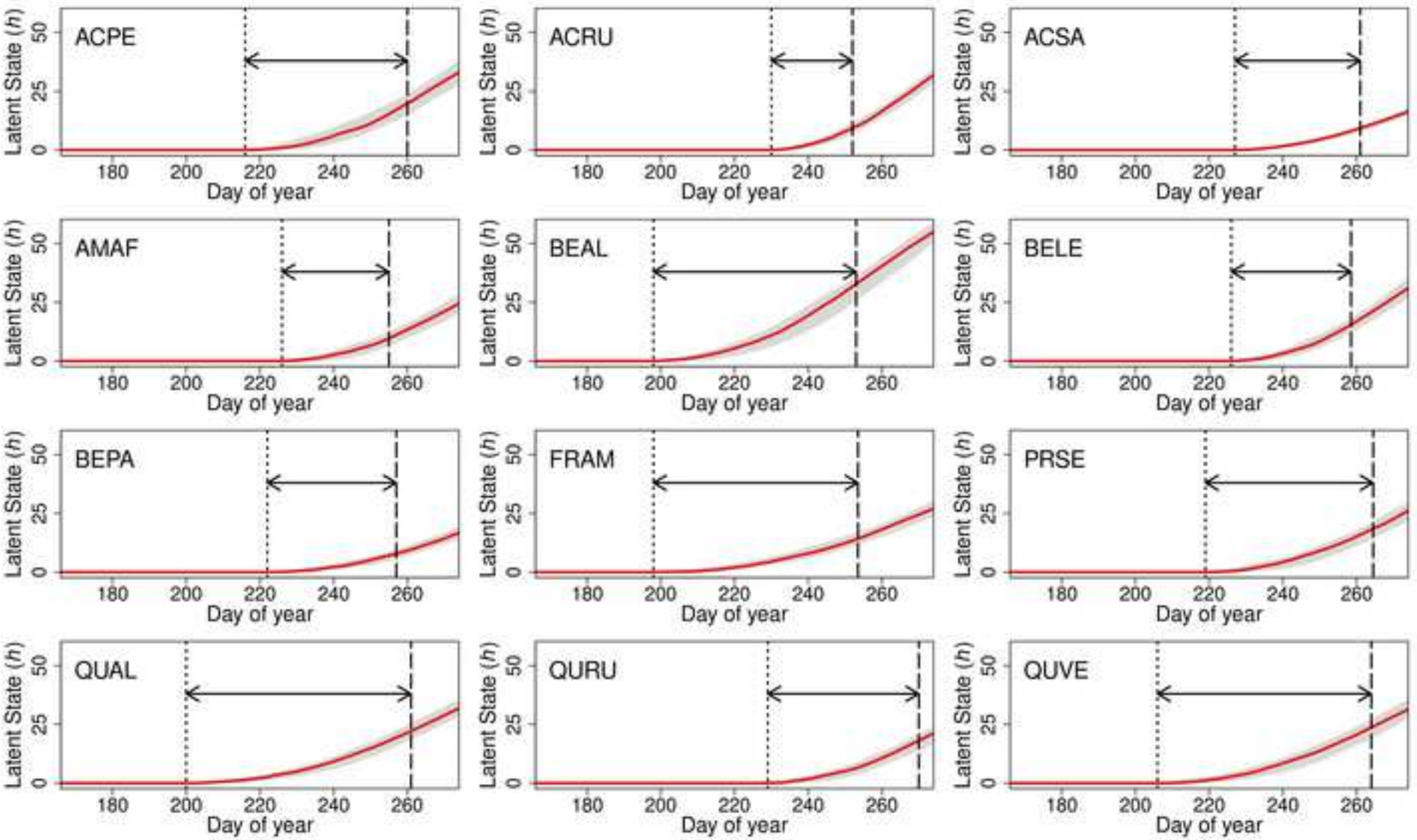

Figure S3

Click here to access/download;Figure;figS3.tif

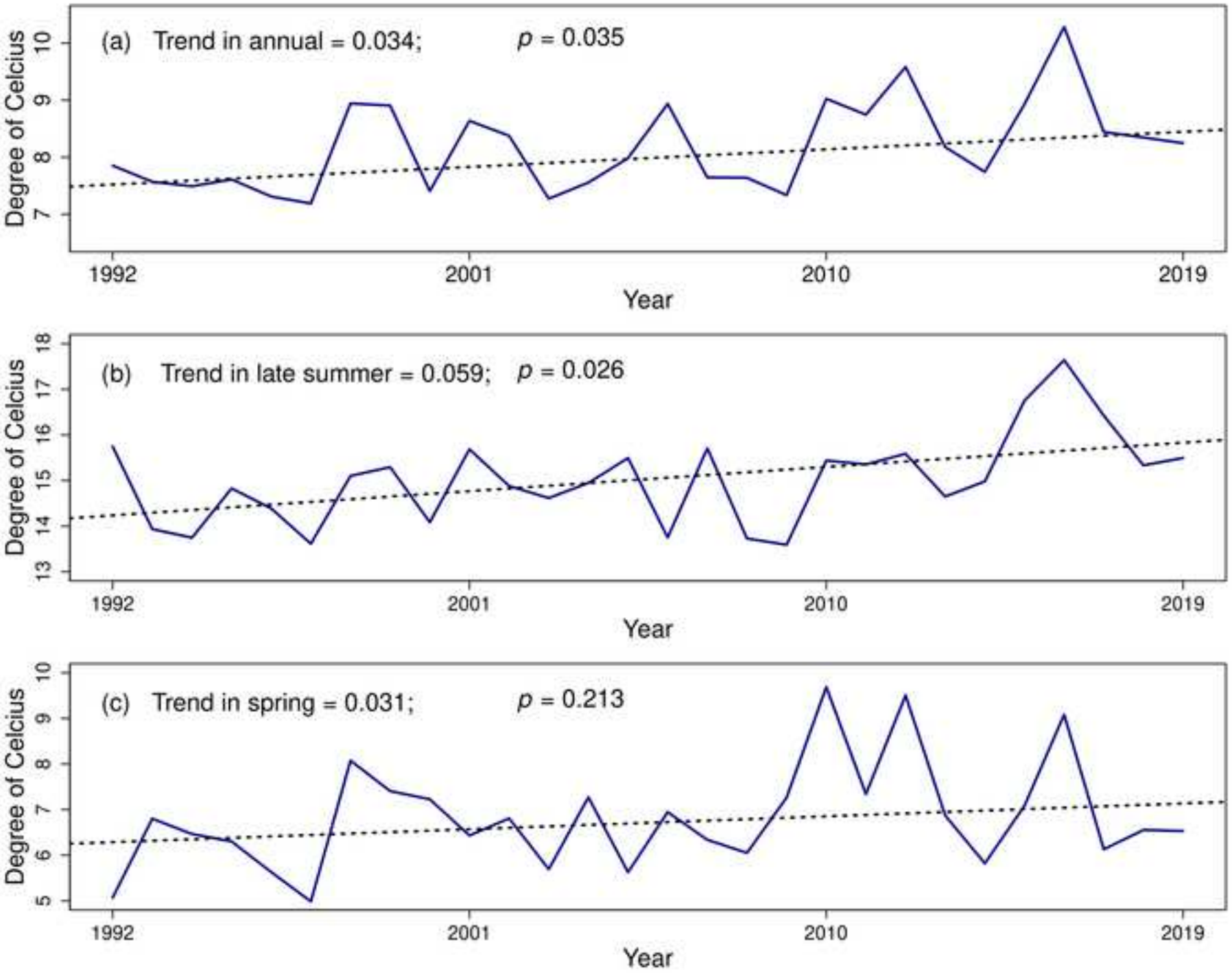

Figure S4

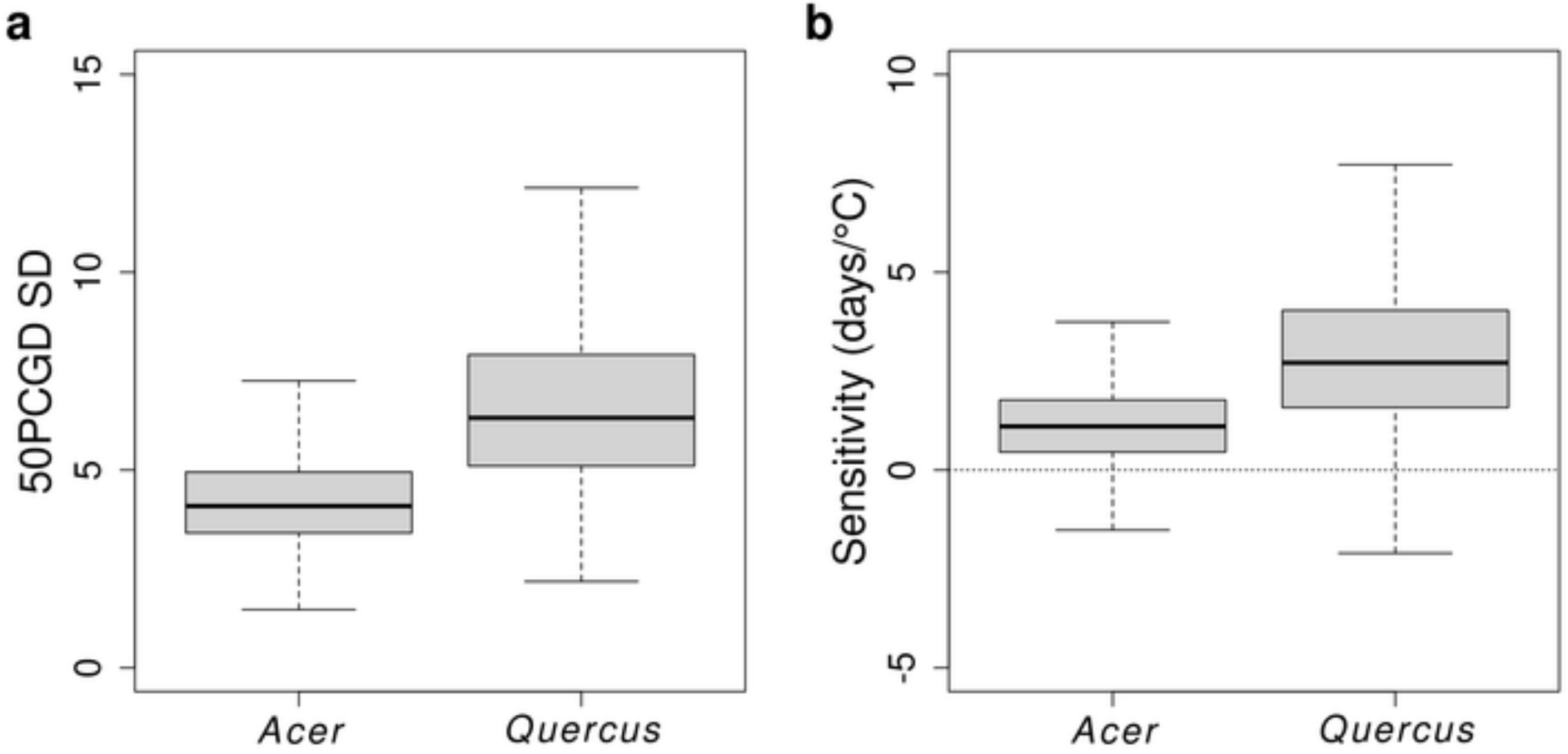

Competing interests

The authors declare no competing interests.